CHAPTER 2

THEORY AND LITERATURE REVIEWS

Thermoelectrics

Thermoelectric phenomena has been described through various theories including the Seebeck effect, Peltier effect, and Thomson effect. These effects are all linked by way of the Kelvin relationship. Moreover, the Figure of Merit and Dimensionless Figure of Merit relating to thermoelectric materials, further describe the properties of these materials. (Rowe, 2006, p. 1–1)

Seebeck Effect

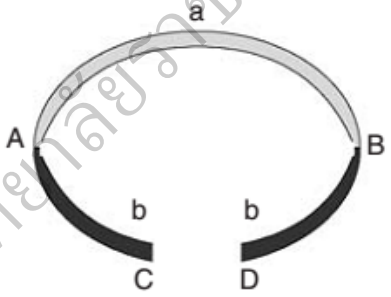

Figure 1 Schematic basic thermocouple

The thermometric phenomena which underlies thermoelectric energy conversion can be conveniently discussed, with reference to the schematic of a thermocouple, as shown in Figure 1. It can be considered as a circuit formed from two dissimilar conductors, a and b (referred to in thermoelectric terms as thermocouple legs, arms, thermoelements, or simply elements and sometimes as pellets by device manufacturers), which are connected electrically in series but thermally in parallel. If the junctions at A and B are maintained at different temperatures T_1 and T_2 and $T_1 > T_2$ an open circuit electromotive force (emf), V is developed between C and D

and given by $V = S(T_1 - T_2)$ or $S = V / \Delta T$, which defines the differential Seebeck coefficient S_{ab} between the elements a and b. For small temperature differences the relationship is linear. The sign of a is positive if the emf causes a current to flow in a clockwise direction around the circuit and is measured in V K^{-1} or more often in μV K^{-1}.

Peltier Effect

In Figure 1, the reverse situation is considered with an external emf source applied across C and D and a current I flows in a clockwise sense around the circuit. Then a rate of heating q occurs at one junction between a and b and a rate of cooling $-q$ occurs at the other. The ratio of I to q defines the Peltier coefficient given by $\prod = I / q$. This is positive if A is heated and B is cooled and is measured in watts per ampere or in volts.

Thomson Effect

The last of the thermoelectric effects, the Thomson effect relates to the rate of generation of reversible heat q, which results from the passage of a current along a portion of a single conductor, along which there is a temperature difference ΔT. Providing the temperature difference is small, $q = \beta I \Delta T$ where β is the Thomson coefficient. The units of β are the same as those of the Seebeck coefficient V K^{-1}. Although the Thomson effect is not of primary importance in thermoelectric devices it should not be neglected in detailed calculations.

The Kelvin Relationships

The above three thermoelectric coefficients are related by the following Kelvin relationships:

$$S_{ab} = \frac{\prod_{ab}}{T} \tag{1}$$

$$\frac{dS_{ab}}{dT} = \frac{\beta_a - \beta_b}{T} \tag{2}$$

These relationships can be derived using irreversible thermodynamics. Their validity has been demonstrated for many thermoelectric materials and it is assumed that they hold for all materials used in thermoelectric applications.

Figure of Merit

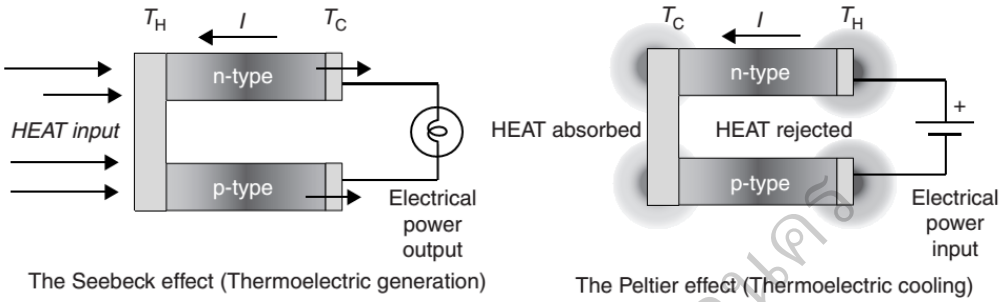

Figure 2 Thermoelectric generator (left); Thermoelectric refrigerator (right)

A thermoelectric converter is a heat engine and like all heat engines it obeys the laws of thermodynamics. If we first consider the converter operating as an ideal generator in which there are no heat losses, the efficiency is defined as the ratio of the electrical power delivered to the load, to the heat absorbed at the hot junction. Expressions for the important parameters in thermoelectric generation can readily be derived by considering the simplest generator, consisting of a single thermocouple with thermo–elements fabricated from *n*– and *p*–type semiconductors, as shown in Figure 2 (left). The efficiency of the generator is given by;

$$\eta = \frac{\text{energysupplied to the load}}{\text{heat energy absorbed at hot junction}} \tag{3}$$

If it is assumed that the electrical conductivities, thermal conductivities, and Seebeck coefficients of a and b are constant within an arm, and that the contact resistances at the hot and cold junctions are negligible compared with the sum of the arm resistance, then the efficiency can be expressed as;

$$\eta = \frac{I^2R}{S_{ab}IT_H} = \frac{I^2R}{\kappa'(T_H - T_C) - \frac{1}{2}I^2R} \tag{4}$$

where κ' is the thermal conductance of a and b in parallel and R is the series resistance of a and b. In thermoelectric materials σ, κ', and S change with temperature, and in both, generation and refrigeration should be taken into account. However, the simple expression obtained for the efficiency can still be employed with an acceptable degree of accuracy, if approximate averages of values are adopted for these parameters over the temperature range of interest. Appropriate allowances can also be made for contact resistance. Efficiency is clearly a function of the ratio of the load resistance to the sum of the generator arm resistances, and at maximum power output it can be shown that;

$$\eta_P = \frac{T_H - T_C}{\frac{3T_H}{2} + \frac{T_C}{2} + \frac{4}{Z_C}} \tag{5}$$

while the maximum efficiency

$$\eta_{max} = \eta_C \gamma \tag{6}$$

where

$$\eta_C = \frac{T_H - T_C}{T_H} \tag{7}$$

$$\gamma = \frac{\sqrt{1 + Z_C \bar{T}} - 1}{\sqrt{1 + Z_C \bar{T}} + \frac{T_C}{T_H}} \tag{8}$$

$$\bar{T} = \frac{T_H + T_C}{2} \tag{9}$$

$$Z_C \text{ (the Figure of Merit of the couple)} = \frac{S_{ab}^2}{R\kappa'} \tag{10}$$

The maximum efficiency is thus the product of the Carnot efficiency, which is clearly less than unity, and γ, which embodies the parameters of the materials. If the geometries of a and b are matched to minimize heat absorption, then;

$$Z_C = \frac{S_{ab}^2}{\sqrt{\kappa_a / \sigma_a} + \sqrt{\kappa_b / \sigma_b})} \tag{11}$$

In practice, the two arms of the junction have similar material constants, in which case the concept of a Figure of Merit for a material is employed and given by;

$$Z = \frac{S^2\sigma}{\kappa} \tag{12}$$

where $S^2\sigma$ is referred to as the electrical power factor.

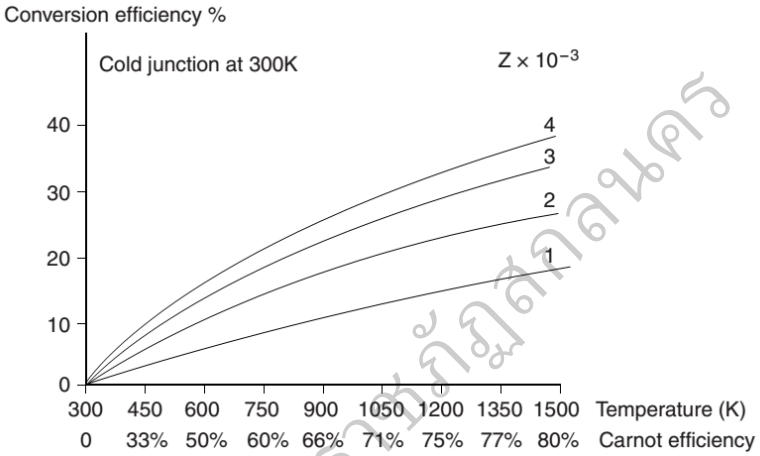

Figure 3 Generating efficiency as a function of temperature and thermocouple material Figure–of–merit

The above relationships have been derived assuming that the thermoelectric parameters which occur in the Figure of merit are independent to temperature. Although generally this is not the case, assuming an average value provides results which are within 10% of the true value. The conversion efficiency as a function of operating temperature difference across a range for values of the material's Figure of merit is displayed in Figure 3. Evidently an increase in temperature difference provides a corresponding increase in available heat for conversion as dictated by the Carnot efficiency. Consequently, large temperature differences are more desirable. As a ballpark figure, a thermocouple fabricated from a thermo–element with an average Figure of Merit of $3\times10^{-3}\,K^{-1}$ would have an efficiency of 20%, when operated over a temperature difference of 500 K.

Thermoelectric Materials

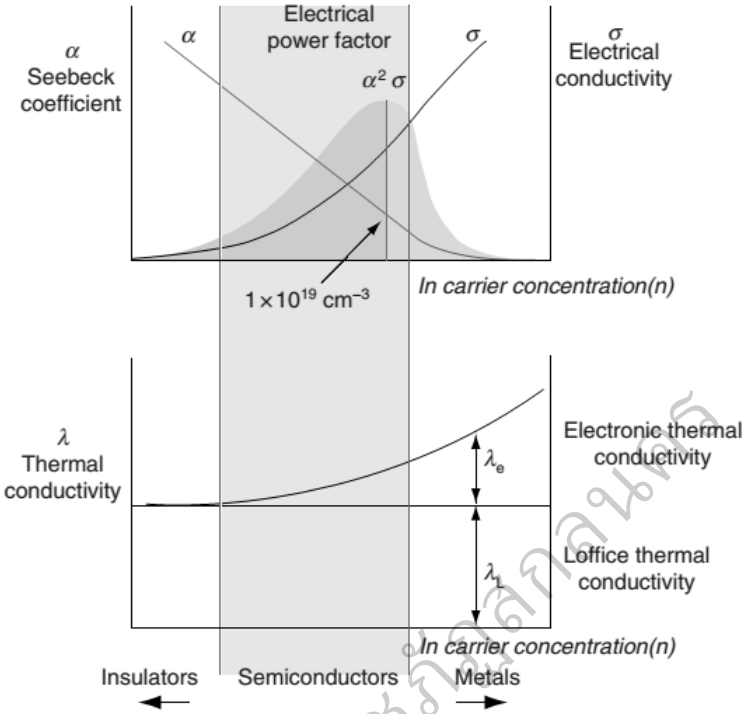

Figure 4 Schematic dependence of electrical conductivity, Seebeck coefficient, power factor, and thermal conductivity on concentration of free carriers

One of the parameters used in the classification of materials is electrical conductivity. Metals have high electrical conductivity, while insulators have very low conductivity which under normal conditions is taken as zero. Semiconductors occupy an intermediate position between the two. Electrical conductivity is a reflection of the charge carrier concentration. All three parameters which occur in the Figure of Merit are functions of carrier concentration. Electrical conductivity increases with an increase in carrier concentration as shown in Figure 4, while the Seebeck coefficient decreases and the electrical power factor maximizes at a carrier concentration of around 10^{25} cm^{-1}. The electronic contribution to the thermal conductivity κ_e, which in thermoelectric materials is generally around 1/3 of the total thermal conductivity, also increases with carrier concentration. Evidently the Figure of Merit optimizes at carrier concentrations which corresponds to semiconductor materials. Consequently, semiconductors are the materials most researched for thermoelectric applications.

Thermoelectric phenomena are exhibited in almost all conducting materials (except for superconductors below T_C). Because the Figure of Merit varies with temperature, a more meaningful measure of performance is the Dimensionless Figure of Merit ZT, where T is absolute temperature. However, only those materials which possess a $\mathrm{ZT} > 0.5$ are usually regarded as thermoelectric materials.

DV-Xα

Adiabatic approximation

The molecules and ions of interest here contain a vast number of nuclei and electrons. The wave function for a molecule is dependent both on the nuclear and electronic coordinates. The first and fundamental approximation to be introduced is the separation of electronic and nuclear motions. This is performed using the so-called "adiabatic approximation" of the molecular wave function. The adiabatic separation leads to two different sets of equations; one governing the electronic wave function an determined by the electronic Schrödinger equation, and the other equation is the associated nuclear wave function given as the solution to a wave equation, in which the electronic energy acts as the potential energy (Born & Huang, 1954; Bixon & Jortner, 1968, p. 715-26; Born & Oppenheimer, 1927, pp.457-484)

Molecular orbital method

The concept of the molecular orbital (MO) method is strongly tied with the idea of the "self-consistent-field" (SCF). The SCF method is one of the most convenient calculations for describing the molecular orbital. In a molecular system consisting of N electrons and many nuclei, the latter being assumed to be *at rest*, each electron will really move in the electronic field produced by all $\mathrm{N}-1$ other electrons and by all the nuclei. If N is rigorous and a very small number, this forms an impossibly difficult problem for a rigorous solution in quantum mechanics, as it would be also impossibly difficult in classical Newtonian mechanics.

Researchers who have studied the electric structure of molecules encountered this difficulty many years ago. They overcame the problem by using a very obvious device. They assumed that the effect of all $N-1$ other electrons could be approximated by averaging the density of them and thereafter using this continuous averaged density. They studied the motion of the one remaining electron in the field of these $N-1$ averaged charges. Then they demanded that the paths of the electrons, so computed, should lead to the same charge density that was assumed in the first place as that of the space charge. The electric field so set up, produced by the electrons in their averaged motions and by any nuclei present, is called a "self-consistent field". The name was introduced by Hartree (1928, pp.89-110). He studied the electrons in an atom as they moved around its nucleus. Independently and at the same time, this same concept of the theory of a self-consistent field was applied to all of these problems. The individual electrons then move in a fixed external field, and at the same time, the same concept was applied to the molecular problem by Hund, Mulliken, Lennard-Jones, and many others. This then formed the basis of theories of electrons in crystals, which can apply the theory of the self-consistent field to all of these problems. The individual electrons then move in a fixed external field and their wave functions, derived from the solution of the Schrödinger equation, are called orbitals.

The effect of this approximation is to reduce the many-body problem from a $3N-$ dimensional one, in three coordinates of all N electrons, to N separate three-dimension problems. This is an enormous simplification. The Schrödinger equation for one of the molecular orbitals is still a difficult one. For an atom, that is Hartree's problem which is quite simple on account of the spherical symmetry. But in the molecule or crystal we no longer have this symmetry, except in the neighborhood of one of the nuclei. Therefore I must gain adequate ways to handle the nonspherical problem of the Schrödinger equation in the molecule.

Hartree approximation

In the 1920s, Bohr's first study of the periodic system of the elements has shown that a "self–consistent field" method is the best approach to solving the many–body problem in the Schrödinger equation. Hartree's first use of the method was based on his intuitiveness.

Consider the many–electron system with atoms or ions of N electrons, surrounding a nucleus at rest, with atomic number Z. Each electron, of course, is acted on electrostatically by the nuclei and all $\mathrm{N}-1$ of the other electrons. In the Hartree's method, the very complicated field exerted by the other electron and nuclei could be replaced by a single potential arising from the averaged charge density of the other electrons and nuclei.

The total wave function Ψ for a many–electron system is then defined as the following product;

$$\Psi = \phi_1(\mathrm{r}_1)\cdot\phi_2(\mathrm{r}_2)\cdots\phi_{\mathrm{N}}(\mathrm{r}_{\mathrm{N}}) \tag{13}$$

where $\phi_i(\mathrm{r}_i)$ is the ith one–electron wave function. This product, a so called "Hartree's product", would indicate that the electrons move independently of each other, which is at the foundation of Hartree's idea. The electronic charge density ρ_i of ith orbital is represented by the following equation;

$$\rho_i(\mathrm{r}) = f_i\phi_i^*(\mathrm{r})\phi_i(\mathrm{r}) \tag{14}$$

where f_i is occupation number of electron to the ith th orbital.

The effective potential in which the ith electron at position r moves is;

$$V_i(\mathrm{r}) = V_N(\mathrm{r}) + V_C(\mathrm{r}) + V_{Xi}(\mathrm{r}) \tag{15}$$

where

$$V_N(\mathrm{r}_1) = -\sum_v \frac{Z_v}{r_{1v}},\quad V_C(\mathrm{r}_1) = -\sum_j \int \frac{\rho_j(\mathrm{r}_2)}{r_{12}}\mathrm{d}\mathrm{r}_2,\quad V_{Xi}(\mathrm{r}_1) = -\int \frac{\rho_i(\mathrm{r}_2)}{r_{12}}\mathrm{d}\mathrm{r}_2 \tag{16}$$

Here the indices i refer to the electrons, the indices v refer to the nuclei, r_{12} is the distance between the electron at position r_1 and the nucleus v, r_{12} is the distance between electrons at position r_1 and r_2, and the ρ_i is the electronic charge density of $i\mathrm{th}$ orbital as is shown in equation (2.2.2). Then V_N is nuclear potential, V_C the electronic repulsive potential arising from all electrons, V_{Xi} the correction term because the electron in one orbital does not act no itself.

Let's apply the variation method of quantum mechanics to the one-electron Schrödinger equation in order to minimize the total energy of the many-electron system. The result will give us the "Hartree's equation" as;

$$\left\{-\frac{1}{2}\nabla_1^2-\sum_v\frac{Z_v}{r_{1v}}+\sum_l\int\phi_l^*(\mathrm{r}_2)\phi_1(\mathrm{r}_2)\frac{1}{\mathrm{r}_{12}}\mathrm{dr}_2-\int\phi_k^*(\mathrm{r}_2)\phi_k(\mathrm{r}_2)\frac{1}{\mathrm{r}_{12}}\mathrm{dr}_2\right\}\phi_k(\mathrm{r}_1)=\varepsilon_k\phi_k(\mathrm{r}_1) \quad (17)$$

where $-\frac{1}{2}\nabla^2$ is the kinetic-energy operator. The SCF method using equation (17) is called the Hartree method.

Hartree-Fock approximation

In the Hartree approximation, the total wave function Ψ for a many-electron system is defined as the Hartree's product, equation (17). It is well known that the antisymmetry of the wave function when the coordinates and spin of two electrons are interchanged, is an expression of Pauli's exclusion principle. The Hartree's product, however, does not have such antisymmetry. To secure the required antisymmetry, it is then necessary to write the many-electron total wave function, Ψ , not in the form of Hartree's product but in the form of the Slater's determinant (Slater, 1974; Slater, 1929, pp.1293-1323);

$$\Psi=\frac{1}{\sqrt{\mathrm{N}!}}\begin{vmatrix}u_1(1) & u_1(2) & \cdots & u_1(N)\\ u_2(1) & u_2(2) & \cdots & u_2(N)\\ \vdots & \vdots & \ddots & \vdots\\ u_N(1) & u_N(2) & \cdots & u_N(1)\end{vmatrix} \quad (18)$$

Enlarge the meaning of the orbitals to include dependence on spins, so that for each electron we can have both an up–spin and down–spin orbital, hence called a "spin orbital". The function Ψ will be equal to zero when two rows or columns of matrix are the same. This means that two electrons cannot occupy the same spin orbital and position.

When applying the variation method so as to minimize the total energy, the resulting one–electron Schrödinger equation is;

$$\left\{-\frac{1}{2}\nabla_1^2-\sum_v\frac{Z_v}{r_{1v}}+\sum_l\int\phi_l^*(\mathrm{r}_2)\phi_1(\mathrm{r}_2)\frac{1}{\mathrm{r}_{12}}\mathrm{dr}_2+V_{Xk}(\mathrm{r}_1)\right\}\phi_k(\mathrm{r}_1)=\varepsilon_k\phi_k(\mathrm{r}_1) \tag{19}$$

where $V_{Xk}(\mathrm{r}_1)$ is the "exchange–correlation potential" as;

$$V_{Xk}(\mathrm{r}_1)=-\frac{\sum_l\int\phi_k^*(\mathrm{r}_1)\phi_1^*(\mathrm{r}_2)\frac{1}{\mathrm{r}_{12}}\phi_l(\mathrm{r}_1)\phi_k(\mathrm{r}_2)\mathrm{dr}_2}{\phi_k^*(\mathrm{r}_1)\phi_k(\mathrm{r}_1)} \tag{20}$$

This term is the potential of a charge whose magnitude is one electron charge removed from a hole surrounding the location of r_1. This charge, which we shall call the "exchange–correlation charge", has the same spin as that of the kth spin orbital and has a charge density at the position of the first electron which is just great enough to neutralize the total electronic charge of spin of ith spin orbital at that point. This hole is often called the "Fermi hole".

The SCF method using equation (18) is called the Hartree–Fock method. This method proves to be the better approximation for molecules and ions than that obtained by the original Hartree method. The last term of equation (19) is, however, obviously much more complicated that the corresponding one in the Hartree method. It's existence in the Hartree–Fock makes any straightforward calculation of molecular orbitals using the Hartree–Fock method quite out of the question, except for the very simplest molecules.

Hartree–Fock–Slater approximation

The Hartree–Fock equation (19) can be applied to atoms without great difficulty, but for crystals it has proven to be unmanageable in most cases. The only term that creates difficulty is the exchange–correlation term. When we multiply the exchange term of equation (19) by the complex conjugate of one orbital, we are dealing with a product of orbitals. Each term leads to what is called a "four–center integral". That is extremely demanding in the amount of computer time and capacity required. Hence, we have to set up a simplified form for the exchange term.

Now fix your attention on an electron with up–spin at a given composition in space. In 1933, Winger and Seitz suggested that this electron of up–spin would repel an electron of down–spin electrostatically, and that this would tend to keep them apart (Wigner & Seitz, 1929, p. 509). Subsequently, the density of other electrons of the same spin fall into zero at the position of the fixed electron, and the integrated deficiency, known as the Fermi hole.

The Hartree–Fock approximation does not take account of this correlation effect. Instead, it only takes account of the exchange–correlation effect that leads to the extreme demand of computing time. In 1951, Slater proposed replacing the exchange–correlation term in equation (20) by the correlation term with the hope that it might make calculation more practical. Then Slater (Slater, 1951, pp.385–390), and later in 1965 W. Kohn and L. J. Sham (Kohn & Sham, 1965, p. A1133), pointed out that the correlation term $V_{X\alpha}$, based on the local spin density approximation (LSDA), would be approximately represented as the following equation;

$$V_{X\alpha\uparrow} = -3\alpha\left(\frac{3}{4\pi}\rho(\mathrm{r})\right)^{\frac{1}{3}} \qquad (21)$$

This approximate potential with a parameter alpha is usually called the $X\alpha$ potential. In the $X\alpha$ method, we can rewrite the expression for the one–electron equation as;

$$\left\{-\frac{1}{2}\nabla_1^2-\sum_v\frac{Z_v}{r_{1v}}+\sum_l\int\rho(\mathrm{r}_2)\frac{1}{r_{12}}\mathrm{dr}_2-3\alpha\left(\frac{3}{4\pi}\rho_\uparrow(\mathrm{r}_1)\right)^{\frac{1}{3}}\right\}\phi_{k\uparrow}(\mathrm{r}_1)=\varepsilon_{k\uparrow}\phi_{k\uparrow}(\mathrm{r}_1) \qquad 22)$$

The SCF method using equation (22) is called "Hartree–Fock–Slater" method.

The LCAO MO approximation

The electronic structure for a molecule is obtained by solving the molecular Schrödinger equation. When applying the variation method to the total energy of electrons ε, the molecular equation results in the one–electron Schrödinger equation;

$$h(\mathrm{r}_1)\phi_k(\mathrm{r}_1)=\varepsilon_k\phi_k(\mathrm{r}_1) \qquad (23)$$

where h is the effective one–electron Hamiltonian, ε_k the eigenvalue of kth orbital. ϕ_k is the wave function of kth molecular orbital, and the unknown function. The molecular orbitals (MO) are in practice always approximated by a linear combination of atomic orbitals (LCAO);

$$\phi_k(\mathrm{r}_1)=\sum_i c_{ik}\chi_i(\mathrm{r}_1) \qquad (24)$$

where c_{ik} is a coefficient dependent on the molecular orbitals, and χ_i is a set of atomic orbitals. This approximation is called the LCAO MO method.

Introducing equation (24) into equation (13) leads to;

$$h(\mathrm{r}_1)\sum_i c_{ik}\chi_i(\mathrm{r}_1)=\varepsilon_k\sum_i c_{ik}\chi_i(\mathrm{r}_1) \qquad (25)$$

Multiply by $\chi_i^*(\mathrm{r}_1)$ and integrate over dr_1:

$$\sum_j c_{jk}\int\chi_i^*(\mathrm{r}_1)h(\mathrm{r}_1)\chi_j(\mathrm{r}_1)\mathrm{dr}_1=\varepsilon_k\sum_j c_{jk}\int\chi_i^*(\mathrm{r}_1)\chi_j(\mathrm{r}_1)\mathrm{dr}_1 \qquad (26)$$

Here below defines a "resonance integral" and "overlap integral" with elements H_{ji} and S_{ij}:

$$H_{ji} = \int \chi_i^*(\mathrm{r}_1) h(\mathrm{r}_1) \chi_j(\mathrm{r}_1) \mathrm{dr}_1, \quad S_{ij} = \int \chi_i^*(\mathrm{r}_1) \chi_j(\mathrm{r}_1) \mathrm{dr}_1 \tag{27}$$

Equation (26) is then transformed to:

$$\sum_j (H_{ij} - \varepsilon_k S_{ij}) c_{jk} = 0 \tag{28}$$

This set of homogeneous linear equations is, generally a "secular equation", equivalent to the following matrix:

$$(\mathrm{H} - \varepsilon \mathrm{S})\mathrm{C} = 0 \tag{29}$$

where H, S, and C is the matrix with the matrix elements H_{ij}, S_{ij}, and c_{jk}.

Fermi–Dirac distribution function

The Fermi–Dirac distribution function (Kittel & Kroemer, 1980) may be derived in several steps by use of a modern approach to statistical mechanics. The notation is such that conventional entropy S is related to the fundamental entropy σ by $\mathrm{S} = k_\mathrm{B}\sigma$, and the Kelvin temperature T is related to the fundamental temperature τ by $\tau = k_\mathrm{B}T$, where k_B is the Boltzmann constant with the value 1.38066×10^{-23} J K. The leading quantities are the entropy, the temperature, the Boltzmann factor, the chemical potential, the Gibbs factor, and the distribution functions. The entropy measures the number of quantum states accessible to a system. A closed system might be in any of these quantum states and with equal probability. The fundamental assumption is that quantum states are either accessible or inaccessible to the system, and the system is equally likely to be in any one accessible state as in any other accessible state. Given g accessible states, the entropy is defined as $\sigma = \log g$. The entropy thus defined will be a function of the energy U, the number of particles N, and the volume V of the system.

The fundamental temperature τ is defined by the relation;

$$\frac{1}{\tau} \equiv \left(\frac{\partial \omega}{\partial U} \right)_{N,V} \tag{30}$$

The use of $1/\tau$ assures that energy will flow from high τ to low τ; a no more complicated relation is needed.

Let a small system with only two states; one at energy 0 and one at energy ε, be placed in thermal contact with a large system that is called the reservoir. The total energy of the combined systems is U_0; when the small system is in the state of energy 0, the reservoir has energy U_0 and will have $g(U_0)$ states accessible to it. By the fundamental assumption, the ratio of the probability of finding the small system with energy ε to the probability of finding it with energy 0 is;

$$\frac{P(\varepsilon)}{P(0)} = \frac{g(U_0 - \varepsilon)}{g(U_0)} \simeq \frac{\exp[\sigma(U_0 - \varepsilon)]}{\exp[\sigma(U_0)]} \tag{31}$$

The reservoir entropy σ may be expanded in a Taylor series;

$$\sigma(U_0 - \varepsilon) \simeq \sigma(U_0) - \varepsilon \left(\frac{\partial \sigma}{\partial U} \right) = \sigma(U_0) - \frac{\varepsilon}{\tau} \tag{32}$$

Temperature is defined by equation (30). Higher order terms in the expansion may be dropped. Cancellation of the term $\exp[\sigma(U_0)]$, which occurs in the numerator and denominator of equation (31) after the substitution of equation (32), leaves us with;

$$\frac{P(\varepsilon)}{P(0)} = \exp(-\tau) \tag{33}$$

This is Boltzmann's result. To show its use, the calculate thermal average energy $\langle \varepsilon \rangle$ of the two–state system in thermal contact with a reservoir at temperature τ;

$$\langle \varepsilon \rangle = \sum_i \varepsilon_i P(\varepsilon_i) = 0 \cdot P(0) + \varepsilon P(\varepsilon) = \frac{\varepsilon \exp(-\varepsilon / \tau)}{1 + \exp(-\varepsilon / \tau)} \tag{34}$$

where the normalization condition is imposed on the sum of the probabilities;

$$P(0)+P(\varepsilon)=1 \tag{35}$$

The argument can be generalized immediately to find the average energy of a harmonic oscillator at temperature τ as in the Planck law.

The most important extension of the theory is to systems that can transfer particles as well as energy with the reservoir. For two systems in diffusive and thermal contact, the entropy will be at maximum with respect to the transfer of particles as well as to the transfer of energy. Not only must $(\partial\sigma/\partial U)_{N,V}$ be equal for the two systems, but $(\partial\sigma/\partial U)_{U,V}$ must also be equal, where N refers to the number of particles of a given species. The new equality condition is the occasion of the chemical potential μ;

$$-\frac{\mu}{\tau}=\left(\frac{\partial\sigma}{\partial U}\right)_{U,V} \tag{36}$$

For two systems in thermal and diffusive contact, $\tau_1=\tau_2$ and $\mu_1=\mu_2$. The sign in equation (36) is chosen to ensure that the direction of particle flow is from high chemical potential to low chemical potential as equilibrium is approached.

The Gibbs factor is an extension of the Boltzmann factor equation (37) and allows us to treat systems that can transfer particles. The simplest example is a system with two states; one with 0 particles and 0 energy, and one with 1 particle and energy ε. The system is in contact with a reservoir at temperature τ and chemical potential μ. We extend equation (32) for the reservoir entropy;

$$\begin{aligned}\sigma(U_0-\varepsilon;N_0-1)&=\sigma(U_0;N_0)-\varepsilon\left(\frac{\partial\sigma}{\partial U_0}\right)-1\cdot\left(\frac{\partial\sigma}{\partial N_0}\right)\\&=\sigma(U_0;N_0)-\frac{\varepsilon}{\tau}+\frac{\mu}{\tau}\end{aligned} \tag{37}$$

By analogy with equation (31), we have the Gibbs factor

$$\frac{P(1,\varepsilon)}{P(0,0)} = \exp[(\mu-\varepsilon)/\tau] \tag{38}$$

This measures the ratio of the probability that the system is occupied by 1 particle at energy ε to the probability that the system is unoccupied, with energy 0. The resultant equation (38) after normalization is readily expressed as;

$$P(1,\varepsilon) = \frac{1}{\exp[(\mu-\varepsilon)/\tau]+1} \tag{39}$$

This is the Fermi–Dirac distribution function.

Charge and heat transport properties

An electron is transported under a small electric field, temperature gradient, and concentration gradient (and thus chemical potential gradient) along the Z direction. Consider an infinitesimal point at height Z. At this point, the distribution function of electrons is *f*, and the number of electrons with an energy between E and $E+\mathrm{d}E$ is $fD(E)\mathrm{d}E$. Since the electric field, temperature gradient and concentration gradient are small, these electrons will have almost the same probability to move toward any direction. Also because the solid angle of a sphere is 4π, the probability for an electron to move in the (θ,ϕ) direction within a solid angle $\mathrm{d}\Omega = \sin\theta \mathrm{d}\theta \mathrm{d}\phi$ will be $\mathrm{d}\Omega/4\pi$. A charge q ($q=-e$ for electrons and $q=+e$ for holes) moving in the (θ,ϕ) direction within a solid angle $\mathrm{d}\Omega$ causes a charge flux of $qv\cos\theta$ and energy flux $Ev\cos\theta$ in the Z direction, where θ is defined as the angel between the velocity vector and the positive Z direction with a range between 0 to π. Hence, the charge flux and energy flux in the Z direction carried by all electrons moving toward the entire sphere surrounding the point are respectively;

$$J_z = \int_{\varphi=0}^{2\pi} \frac{1}{4\pi} d\varphi \int_{\theta=0}^{\pi} \sin\theta\cos\theta d\theta \int_{E=0}^{\infty} fD(E)qvdE \tag{40}$$

$$J_{E_Z} = \int_{\varphi=0}^{2\pi} \frac{1}{4\pi} d\varphi \int_{\theta=0}^{\pi} \sin\theta\cos\theta d\theta \int_{E=0}^{\infty} fD(E)EvdE \tag{41}$$

With the relaxation–time approximation, the Boltzmann transport equation for electrons take the following form;

$$\frac{\partial f}{\partial t}+\vec{v}\cdot\nabla f+q\vec{E}\cdot\frac{\partial f}{\partial \vec{p}}=\frac{f_0-f}{\tau} \tag{42}$$

where $q=-e$ for electrons and $q=+e$ for holes. For the steady state case with a small temperature/concentration gradient and electric field in the Z direction only, the variation of the distribution function in time is much smaller than that in space, or $\frac{\partial f}{\partial t}<<\vec{v}\cdot\nabla f$, so that we can assume $\frac{\partial f}{\partial t}\sim 0$. The temperature gradient and electric field is small so that the deviation from an equilibrium distribution f_0 is small, i.e. $f_0-f\ll f_0,\ \nabla f\approx\nabla f_0,$ and $\frac{\partial f}{\partial \vec{p}}\approx\frac{\partial f_0}{\partial \vec{p}}=\frac{\partial f_0}{\partial E}\frac{dE}{d\vec{p}}=\vec{v}\frac{\partial f_0}{\partial E}$. With these assumptions, equation (41) becomes

$$\vec{v}\cdot\left(\nabla f_0+q\vec{E}\frac{\partial f_0}{\partial E}\right)=\frac{f_0-f}{\tau} \tag{43}$$

The equilibrium distribution of electrons is the Fermi–Dirac distribution**;**

$$f_0(\vec{k})=\frac{1}{\exp\left(\frac{E(\vec{k})-\mu}{k_{\mathrm{B}}T}\right)+1}=\frac{1}{\exp(\eta)+1};\ \ \eta\equiv\frac{E-\mu}{k_{\mathrm{B}}T} \tag{45}$$

where μ is the chemical potential that depends strongly on carrier concentration and weakly on temperature. Both *E* and μ are measured from the band edge (e.g. E_C for conduction band). This reference system essentially sets $E_C=0$ at different locations, although the absolute value of E_C measured from a global reference varies at different locations ($\mu=E_{\mathrm{F}}$ in Chen). In this reference system corresponding to Fig. 6.9b in Chen, the same quantum state $\vec{k}=(k_x,\ k_y,\ k_z)$ has the same energy $E(\vec{k})=E(\vec{k})-E_C=\frac{\hbar^2(k_x^2+k_y^2+k_z^2)}{2m}$ at different locations. Hence this reference system yields the gradient $\nabla E(\vec{k})=0$, simplifying the following derivation. If we use a global reference level as our zero energy reference point, as in three dimension, the quantum state $\vec{k}=(k_x,\ k_y,\ k_z)$ has different energy

$E(\vec{k}) = \frac{\hbar^2}{2m}(k_x^2 + k_y^2 + k_z^2) + E_C$ because E_C changes with locations. In this case, $\nabla E(\vec{k}) = \nabla E_C \neq 0$, makes the following derivation somewhat inconvenient. However, both reference systems will yield the same result.

From equation (43),

$$\frac{\partial f_0}{\partial E} = \frac{df_0}{d\eta}\frac{\partial \eta}{\partial E} = \frac{df_0}{d\eta}\frac{1}{k_B T}; \quad \text{or} \quad \frac{df_0}{d\eta} = k_B T \frac{\partial f_0}{\partial E} \tag{44}$$

From equation (44),

$$\nabla f_0 = \frac{df_0}{d\eta}\nabla\eta = k_B T \frac{\partial f_0}{\partial E}\nabla\eta \tag{45}$$

Also because $\nabla E(\vec{k}) = 0$ for the reference system, then using;

$$\nabla\eta = \frac{1}{k_B T}(\nabla E(\vec{k}) - \nabla\mu) - \frac{E-\mu}{k_B T^2}\nabla T = \frac{1}{k_B T}\nabla\mu - \frac{E-\mu}{k_B T^2}\nabla T \tag{46}$$

From equation (45–46),

$$\nabla f_0 = -\frac{\partial f_0}{\partial E}\left(\nabla\mu + \frac{E-\mu}{T}\nabla T\right) \tag{47}$$

Combining equation (42) and (47) obtains

$$\vec{v}\cdot\left(-\nabla\mu - \frac{E-\mu}{T}\nabla T + q\vec{E}\right)\frac{\partial f_0}{\partial E} = \frac{f_0 - f}{\tau} \tag{48}$$

Note that

$$\vec{E} = -\nabla\varphi_e \tag{49}$$

where φ_e is the electrostatic potential (also called electrical potential, which is the potential energy per unit of charge associated with a time–invariant electric field $\vec{E}$); From equation (48) and (49), obtain**;**

$$\vec{v}\cdot\left(-\nabla\mu - \frac{E-\mu}{T}\nabla T - q\nabla\phi_e\right)\frac{\partial f_0}{\partial E} = \frac{f_0 - f}{\tau} \tag{50}$$

From equation (50), we obtain**;**

$$f = f_0 - \tau\vec{v}\cdot\left(-\nabla\Phi - \frac{E-\mu}{T}\nabla T\right)\frac{\partial f_0}{\partial E} \tag{51}$$

where $\Phi = \mu + q\phi_e$, is the electrochemical potential that combines the chemical potential and electrostatic potential energy. This definition of the electrochemical potential is the definition in Chen's text multiplied by a factor of q. Both definitions are used in the literature, though the definition here is used more widely. Electrochemical potential is the driving force for current flow, which can be caused by either the gradient in chemical potential (e.g. due to the gradient in carrier concentration) or the gradient in electrostatic potential (i.e. electric field). When you measure voltage ΔV across a solid using a voltmeter, you actually measure the electrochemical potential difference $\Delta\Phi$ per unit charge between the two ends of the solid, i.e. $\Delta V = \Delta\Phi / q$. If there is no temperature gradient or concentration gradient in the solid, the measured voltage equals $\Delta\varphi_e$. In the current case all the gradients and $\vec{E}$ are in the Z direction, so from equation (50),

$$\begin{aligned} f &= f_0 - \tau v\cos\theta\left(-\frac{d\mu}{dZ} - \frac{E-\mu}{T}\frac{dT}{dZ} + qE_z\right)\frac{\partial f_0}{\partial E} \\ &= f_0 - \tau v\cos\theta\left(-\frac{d\Phi}{dZ} - \frac{E-\mu}{T}\frac{dT}{dZ}\right)\frac{\partial f_0}{\partial E} \end{aligned} \tag{52}$$

Combining equation (40) and (52), obtains the charge flux and energy flux respectively;

$$\begin{aligned} J_z = &\int_{\varphi=0}^{2\pi}\frac{1}{4\pi}d\varphi\int_{\theta=0}^{\pi}\sin\theta\cos\theta d\theta\int_{E=0}^{\infty}f_0 D(E)qvdE \\ &+\int_{\varphi=0}^{2\pi}\frac{1}{4\pi}d\varphi\int_{\theta=0}^{\pi}\sin\theta\cos^2\theta d\theta\int_{E=0}^{\infty}\frac{\partial f_0}{\partial E}D(E)qv^2\tau\left(\frac{d\mu}{dZ}+\frac{E-\mu}{T}\frac{dT}{dZ}-qE_z\right)dE \end{aligned} \tag{53a}$$

and

$$\begin{aligned} J_{E_Z} = &\int_{\varphi=0}^{2\pi}\frac{1}{4\pi}d\varphi\int_{\theta=0}^{\pi}\sin\theta\cos\theta d\theta\int_{E=0}^{\infty}f_0 D(E)EvdE \\ &+\int_{\varphi=0}^{2\pi}\frac{1}{4\pi}d\varphi\int_{\theta=0}^{\pi}\sin\theta\cos^2\theta d\theta\int_{E=0}^{\infty}\frac{\partial f_0}{\partial E}D(E)Ev^2\tau\left(\frac{d\mu}{dZ}+\frac{E-\mu}{T}\frac{dT}{dZ}-qE_z\right)dE \end{aligned} \tag{53b}$$

Note that the first term on the right hand side of equation (53) is zero and the second term yields;

$$J_z = \frac{1}{3}\int_{E=0}^{\infty} \frac{\partial f_0}{\partial E} D(E) q v^2 \tau \left(\frac{d\mu}{dZ} + \frac{E-\mu}{T}\frac{dT}{dZ} - qE_z \right) dE \tag{54a}$$

$$J_{E_Z} = \frac{1}{3}\int_{E=0}^{\infty} \frac{\partial f_0}{\partial E} D(E) E v^2 \tau \left(\frac{d\mu}{dZ} + \frac{E-\mu}{T}\frac{dT}{dZ} - qE_z \right) dE \tag{54b}$$

Note that

$$E = \frac{1}{2} m v^2 \tag{55}$$

Use equation (55) to eliminate v in equation (56), and obtain;

$$\begin{aligned} J_z &= \frac{2q}{3m}\int_{E=0}^{\infty} \frac{\partial f_0}{\partial E} D(E) E \tau \left(\frac{d\mu}{dZ} + \frac{E-\mu}{T}\frac{dT}{dZ} - qE \right)_z dE \\ &= \frac{2q}{3m}\int_{E=0}^{\infty} \frac{\partial f_0}{\partial E} D(E) E \tau \left(\frac{d\Phi}{dZ} + \frac{E-\mu}{T}\frac{dT}{dZ} \right) dE \end{aligned} \tag{56a}$$

$$J_{E_Z} = \frac{2}{3m}\int_{E=0}^{\infty} \frac{\partial f_0}{\partial E} D(E) E^2 \tau \left(\frac{d\mu}{dZ} + \frac{E-\mu}{T}\frac{dT}{dZ} - qE_z \right) dE \tag{56b}$$

The energy flux from equation (56b) can be broken up into two terms as follows;

$$\begin{aligned} J_{E_Z} &= \frac{2}{3m}\int_{E=0}^{\infty} \frac{\partial f_0}{\partial E} D(E) E^2 \tau \left(\frac{d\mu}{dZ} + \frac{E-\mu}{T}\frac{dT}{dZ} - qE_z \right) dE \\ &= \frac{2}{3m}\int_{E=0}^{\infty} \frac{\partial f_0}{\partial E} D(E) E (E-\mu) \tau \left(\frac{d\mu}{dZ} + \frac{E-\mu}{T}\frac{dT}{dZ} - qE_z \right) dE \\ &\quad + \mu \frac{2}{3m}\int_{E=0}^{\infty} \frac{\partial f_0}{\partial E} D(E) E \tau \left(\frac{d\mu}{dZ} + \frac{E-\mu}{T}\frac{dT}{dZ} - qE_z \right) dE \\ &= \frac{2}{3m}\int_{E=0}^{\infty} \frac{\partial f_0}{\partial E} D(E) E (E-\mu) \tau \left(\frac{d\mu}{dZ} + \frac{E-\mu}{T}\frac{dT}{dZ} - qE_z \right) dE + \frac{\mu J_Z}{q} \\ &= \frac{2}{3m}\int_{E=0}^{\infty} \frac{\partial f_0}{\partial E} D(E) E (E-\mu) \tau \left(\frac{d\Phi}{dZ} + \frac{E-\mu}{T}\frac{dT}{dZ} \right) dE + \frac{\mu J_Z}{q} \end{aligned} \tag{57}$$

where J_Z is the current density or charge flux given by equation (56a). At temperature $T = 0$K, the first term on the right hand side of equation (57) is zero, so that the energy flux at $T = 0$K is;

$$J_{E_z}(T=0K)=\frac{\mu J_Z}{q} \tag{58}$$

Because electrons don't carry any thermal energy at $T=0$ K, the thermal energy flux or heat flux carried by the electrons at $T\neq 0$ is;

$$\begin{aligned} J_{q_Z}(T) &= J_{E_Z}(T)-J_{E_Z}(T=0) \\ &= \frac{2}{3m}\int_{E=0}^{\infty}\frac{\partial f_0}{\partial E}D(E)E(E-\mu)\tau\left(\frac{d\Phi}{dZ}+\frac{E-\mu}{T}\frac{dT}{dZ}\right)dE \end{aligned} \tag{59}$$

Equations (2.4.17a) and (2.4.20) can be rearranged as;

$$J_z = L_{11}\left(-\frac{1}{q}\frac{d\Phi}{dZ}\right)+L_{12}\left(-\frac{dT}{dZ}\right) \tag{60a}$$

$$J_{q_z} = L_{21}\left(-\frac{1}{q}\frac{d\Phi}{dZ}\right)+L_{22}\left(-\frac{dT}{dZ}\right) \tag{60b}$$

where

$$L_{11}=-\frac{2q^2}{3m}\int_{E=0}^{\infty}\frac{\partial f_0}{\partial E}D(E)E\tau dE \tag{61a}$$

$$L_{12}=-\frac{2q}{3mT}\int_{E=0}^{\infty}\frac{\partial f_0}{\partial E}D(E)E(E-\mu)\tau dE \tag{61b}$$

$$L_{21}=-\frac{2q}{3m}\int_{E=0}^{\infty}\frac{\partial f_0}{\partial E}D(E)E(E-\mu)\tau dE = TL_{12} \tag{61c))}$$

$$L_{22}=-\frac{2}{3mT}\int_{E=0}^{\infty}\frac{\partial f_0}{\partial E}D(E)E(E-\mu)^2\tau dE \tag{61d}$$

In the case of a zero temperature gradient and zero carrier concentration gradient, $\frac{dT}{dZ}=0$ and $\frac{d\mu}{dZ}=0$, equation (60a) becomes;

$$J_z = L_{11}\left(-\frac{1}{q}\frac{d\Phi}{dZ}\right)=L_{11}\left(-\frac{1}{q}\frac{d\mu}{dZ}+E_z\right)=L_{11}E_z \tag{62}$$

The electrical conductivity is defined as;

$$\sigma\equiv\frac{J_z}{E_z}=L_{11}=-\frac{2q^2}{3m}\int_{E=0}^{\infty}\frac{\partial f_0}{\partial E}D(E)E\tau dE \tag{63}$$

Seebeck coefficient

In the case of a non–zero temperature gradient along the Z direction, a thermoelectric voltage can be measured between the two ends of the solid with an open loop electrometer, i.e. $J_z = 0$. Hence from equation (60a) comes;

$$J_z = L_{11}\left(-\frac{1}{q}\frac{d\Phi}{dZ}\right) + L_{12}\left(-\frac{dT}{dZ}\right) = 0 \tag{64}$$

Therefore

$$\frac{\left(\frac{d\Phi}{dZ}\right)}{\left(\frac{dT}{dZ}\right)} = -\frac{qL_{12}}{L_{11}} \tag{65}$$

As discussed above, the voltage that the electrometer measure between the two ends of the solid is $\Delta V = \Delta\Phi / q$. Similarly, $dV = d\Phi / q$. The Seebeck coefficient is defined as the ratio between the voltage gradient and the temperature gradient for an open loop configuration with zero net current flow

$$\begin{aligned} S = -\frac{\left(\frac{dV}{dZ}\right)}{\left(\frac{dT}{dZ}\right)} &= -\frac{1}{q}\frac{\left(\frac{d\Phi}{dZ}\right)}{\left(\frac{dT}{dZ}\right)} = \frac{L_{12}}{L_{11}} \\ &= \frac{1}{qT}\left(\frac{\int_{E=0}^{\infty}\frac{\partial f_0}{\partial E}D(E)E(E-\mu)\tau dE}{\int_{E=0}^{\infty}\frac{\partial f_0}{\partial E}D(E)E\tau dE}\right) \\ &= -\frac{1}{qT}\left(\mu - \frac{\int_{E=0}^{\infty}\frac{\partial f_0}{\partial E}D(E)E^2\tau dE}{\int_{E=0}^{\infty}\frac{\partial f_0}{\partial E}D(E)E\tau dE}\right) \end{aligned} \tag{66}$$

Combining equation (66), (63), and (60a), produces;

$$J_z = \sigma\left(-\frac{1}{q}\frac{d\Phi}{dZ}\right) + \sigma S\left(-\frac{dT}{dZ}\right)$$

The scattering means free time depends on the energy, and assumes;

$$\tau = \tau_0 E^r \tag{67}$$

where τ_0 is a constant independent of E and E is measured from the band edge for either electrons or holes, the density of states;

$$D(E) = \frac{(2m)^{3/2}}{2\pi^2\hbar^3} E^{1/2} \tag{68}$$

Combine equation (66) and (68);

$$S = -\frac{1}{qT}\left(\mu - \frac{\int_{E=0}^{\infty} \frac{\partial f_0}{\partial E} D(E)E^2\tau dE}{\int_{E=0}^{\infty} \frac{\partial f_0}{\partial E} D(E)E\tau dE} \right) = -\frac{1}{qT}\left(\mu - \frac{\int_{E=0}^{\infty} \frac{\partial f_0}{\partial E} E^{2+r+1/2} dE}{\int_{E=0}^{\infty} \frac{\partial f_0}{\partial E} E^{1+r+1/2} dE} \right) \tag{69}$$

The integrals in equation (69) can be simplified using the product rule;

$$\int_{E=0}^{\infty} \frac{\partial f_0}{\partial E} E^s dE = f_0 E^s \,|_0^{\infty} - s \int_{E=0}^{\infty} f_0 E^{s-1} dE = -s \int_{E=0}^{\infty} f_0 E^{s-1} dE \tag{70}$$

Using equation (70) to reduce equation (69) to

$$S = -\frac{1}{qT}\left(\mu - \frac{(r+5/2)\int_{E=0}^{\infty} f_0 E^{r+3/2} dE}{(r+3/2)\int_{E=0}^{\infty} f_0 E^{r+1/2} dE} \right) \tag{71}$$

The two integrals in equation (71) can be simplified with the reduced energy $\zeta = E / k_B T$

$$\begin{aligned} \int_{E=0}^{\infty} f_0(E,\mu) E^n dE &= (k_B T)^{n+1} \int_0^{\infty} f_0(\zeta,\eta)\zeta^n d\zeta \\ &= (k_B T)^{n+1} F_n(\eta); \quad \eta = \mu / k_B T \end{aligned} \tag{72}$$

where the Fermi–Dirac integral is defined as

$$F_n(\eta) = \int_0^{\infty} f_0(\zeta,\eta)\zeta^n d\zeta \tag{73}$$

Use equation (72) to reduce equation (71) to

$$S=-\frac{1}{qT}\left(\mu-k_{\mathrm{B}}T\frac{\left(r+\frac{5}{2}\right)F_{r+3/2}(\eta)}{\left(r+\frac{3}{2}\right)F_{r+1/2}(\eta)}\right)=-\frac{k_{\mathrm{B}}}{q}\left(\eta-\frac{\left(r+\frac{5}{2}\right)F_{r+3/2}(\eta)}{\left(r+\frac{3}{2}\right)F_{r+1/2}(\eta)}\right) \quad (74)$$

Seebeck coefficient for metals

For metals with $\eta=\mu/k_{\mathrm{B}}T>>0$, the Fermi–Dirac integral can be expressed in the form of a rapidly converging series;

$$\begin{aligned}F_n(\eta)&=\int_0^\infty f_0\zeta^n d\zeta=-\frac{1}{n+1}\int_0^\infty\frac{\partial f_0}{\partial\zeta}\zeta^{n+1}d\zeta\\&=-\frac{1}{n+1}\int_0^\infty\frac{\partial f_0}{\partial\zeta}\left(\eta^{n+1}+\sum_{m=1}^{\infty}\left.\frac{d^m\left(\zeta^{n+1}\right)}{d\zeta^m}\right|_{\zeta=\eta}\frac{(\zeta-\eta)^m}{m!}\right)d\zeta\\&=-\frac{1}{n+1}\int_0^\infty\frac{\partial f_0}{\partial\zeta}\left(\eta^{n+1}+(n+1)\eta^n(\zeta-\eta)+(n+1)n\eta^{n-1}\frac{(\zeta-\eta)^2}{2}+\ldots\right)d\zeta\\&=\frac{\eta^{n+1}}{n+1}+n\eta^{n-1}\frac{\pi^2}{6}+\ldots\end{aligned} \quad (75)$$

If we use only the first two terms of equation (75) to express the two Fermi–Dirac integrals in equation (74), we obtain the following ($q=-e$ for electrons in metals);

$$\begin{aligned}S&=-\frac{k_{\mathrm{B}}}{q}\left(\eta-\frac{\left(r+\frac{5}{2}\right)F_{r+3/2}(\eta)}{\left(r+\frac{3}{2}\right)F_{r+1/2}(\eta)}\right)\\&=\frac{k_{\mathrm{B}}}{e}\left(\frac{\eta\left(r+\frac{3}{2}\right)F_{r+1/2}(\eta)-\left(r+\frac{5}{2}\right)F_{r+3/2}(\eta)}{\left(r+\frac{3}{2}\right)F_{r+1/2}(\eta)}\right)\end{aligned}$$

$$= \frac{k_B}{e}\left(\frac{\eta\left(r+\frac{3}{2}\right)\left(\frac{\eta^{r+3/2}}{r+\frac{3}{2}}+\left(r+\frac{1}{2}\right)\eta^{r-1/2}\frac{\pi^2}{6}\right)-\left(r+\frac{5}{2}\right)\left(\frac{\eta^{r+5/2}}{r+\frac{5}{2}}+\left(r+\frac{3}{2}\right)\eta^{r+1/2}\frac{\pi^2}{6}\right)}{\left(r+\frac{3}{2}\right)\frac{\eta^{r+3/2}}{r+\frac{3}{2}}} \right)$$

$$= -\frac{\pi^2 k_B}{3e}\left(\frac{k_B T}{\mu}\right)\left(\frac{3}{2}+r\right)$$

$$S_{\text{metal}} = -\frac{\pi^2 k_B}{3e}\left(\frac{k_B T}{E_F}\right)\left(\frac{3}{2}+r\right) \tag{76}$$

This value can be either positive or negative depending on r, or how the scattering rate depends on electron energy. This values also ignores the weak temperature dependence of μ and assumes $\mu = E_F$, the Fermi level that is the highest energy occupied by electrons at 0 K in a metal.

Seebeck coefficient for non-degenerate semiconductors

In non-degenerate semiconductors, μ is located within the band gap with a distance from the conduction or valence band edges larger than $k_B T$, so that $\frac{E-\mu}{k_B T} = \zeta - \eta > 3$. This is true for both electrons in the conduction band and holes in the valence band. For holes in the valence band, the energy is higher at a position further down and below the valence band edge.

When $\frac{E-\mu}{k_B T} = \zeta - \eta > 3$, the Fermi-Dirac integrals become;

$$F_n(\eta) = \int_0^\infty f_0(\zeta,\eta)\zeta^n d\zeta = \int_0^\infty \frac{1}{\exp(\zeta-\eta)+1}\zeta^n d\zeta \approx \int_0^\infty \frac{1}{\exp(\zeta-\eta)}\zeta^n d\zeta$$

$$= \exp(\eta)\int_0^\infty \exp(-\zeta)\zeta^n d\zeta = \exp(\eta)\Gamma(n+1) \tag{77}$$

where the gamma function has the property

$$\Gamma(n+1) = \int_0^\infty \exp(-\zeta)\zeta^n d\zeta = n\Gamma(n) \tag{78}$$

Equation (78) can be used to reduce equation (74) to;

$$S = -\frac{k_B}{q}\left(\eta - \frac{\left(r+\frac{5}{2}\right)\exp(\eta)\Gamma\left(r+\frac{5}{2}\right)}{\left(r+\frac{3}{2}\right)\exp(\eta)\Gamma\left(r+\frac{3}{2}\right)}\right)$$

$$= -\frac{k_B}{q}\left(\eta - \left(r+\frac{5}{2}\right)\right)$$

$$= -\frac{1}{qT}\left(\mu - k_B T\left(r+\frac{5}{2}\right)\right)$$

$$S_{semi} = -\frac{1}{qT}\left(E_F - k_B T\left(r+\frac{5}{2}\right)\right) \qquad (79)$$

In this equation, μ is measured from the conduction band edge E_C for electrons and from the valence band edge E_V for holes. Located within the band gap μ is negative for electrons, and is also negative for holes, because the hole energy is higher when the energy level is moved further down. Also $q = -e$ for electrons and $q = +e$ for holes, so that the Seebeck coefficient is negative for electrons in the conduction band and positive for holes in the valence band. If μ is measured from a global reference instead of the band edge as the zero energy point, equation (79) can be expressed for electrons and holes separately;

$$S_e = -\frac{1}{eT}(E_c - \mu + (r+5/2)k_B T) < 0, \qquad \text{for electrons} \qquad (80)$$

$$S_h = \frac{1}{eT}(\mu - E_v + (r+5/2)k_B T) > 0, \qquad \text{for holes} \qquad (81)$$

The effective Seebeck coefficient in nondegenerate semiconductors receive contributions from both electrons and holes, i.e.

$$S = \frac{n\mu_e S_e + p\mu_h S_h}{n\mu_e + p\mu_h} \qquad (82)$$

where n and p are electron and hole concentrations, respectively, and μ_e and μ_h represent the mobility of electrons and holes, respectively. The mobility is defined in the following section on Wiedemann–Franz law.

Electrons thermal conductivity

From equation (60a);

$$-\frac{1}{q}\frac{d\Phi}{dZ}=-\frac{L_{12}}{L_{11}}\left(-\frac{dT}{dZ}\right)+\frac{1}{L_{11}}J_z \tag{83}$$

Use equation (83) to eliminate $\frac{d\Phi}{dZ}$ from equation (60b) and obtain;

$$J_{q_z}=\frac{L_{21}}{L_{11}}J_Z+\left(L_{22}-\frac{L_{12}L_{21}}{L_{11}}\right)\left(-\frac{dT}{dZ}\right)=\Pi J_Z+k_e\left(-\frac{dT}{dZ}\right) \tag{84}$$

The Peltier coefficient Π and thermal conductivity k_e are defined in the following equations. In the case of zero current $J_Z=0$ and non-zero temperature gradient along the Z direction;

$$J_{q_Z}=\left(L_{22}-\frac{L_{12}L_{21}}{L_{11}}\right)\left(-\frac{dT}{dZ}\right) \tag{85}$$

The thermal conductivity of electrons;

$$k_e=-\frac{J_{q_Z}}{\frac{dT}{dZ}}=\left(L_{22}-\frac{L_{12}L_{21}}{L_{11}}\right)=\left(L_{22}-L_{21}S\right)$$

$$=\frac{2}{3mT}\left(\frac{\left(\int_{E=0}^{\infty}\frac{\partial f_0}{\partial E}D(E)E(E-\mu)\tau dE\right)^2}{\int_{E=0}^{\infty}\frac{\partial f_0}{\partial E}D(E)E\tau dE}-\int_{E=0}^{\infty}\frac{\partial f_0}{\partial E}D(E)E(E-\mu)^2\tau dE\right) \tag{86}$$

Equation (86) can be reduced to the following equation by expanding the ($E-\mu$) term in the two integrals;

$$k_e=\frac{2}{3mT}\left(\frac{\left(\int_{E=0}^{\infty}\frac{\partial f_0}{\partial E}D(E)E^2\tau dE\right)^2}{\int_{E=0}^{\infty}\frac{\partial f_0}{\partial E}D(E)E\tau dE}-\int_{E=0}^{\infty}\frac{\partial f_0}{\partial E}D(E)E^3\tau dE\right) \tag{87}$$

For metals, S is usually very small so that from equation (86);

$$k_e = \left(L_{22} - L_{21}S\right) \approx L_{22} = -\frac{2}{3mT}\int_{E=0}^{\infty} \frac{\partial f_0}{\partial E} D(E)E(E-\mu)^2 \tau dE \qquad (88)$$

Note that

$$\frac{\partial f_0}{\partial T} = \frac{df_0}{d\eta}\frac{\partial \eta}{\partial T} = -\frac{df_0}{d\eta}\frac{E-\mu}{k_B T^2} \qquad (89)$$

Comparing equation (89) with equation (44) produces;

$$\frac{\partial f_0}{\partial E} = -\frac{T}{E-\mu}\frac{\partial f_0}{\partial T} \qquad (90)$$

Combining equation (89) and (90) gives;

$$k_e = \frac{2}{3m}\int_{E=0}^{\infty} \frac{\partial f_0}{\partial T} D(E)E(E-\mu)\tau dE \qquad (91)$$

Then use $E = mv^2/2$ to rewrite equation (91) as;

$$k_e = \frac{1}{3}\int_{E=0}^{\infty} \frac{\partial f_0(E)}{\partial T} D(E)v^2(E-\mu)\tau dE \qquad (92)$$

When E is far away from μ, $f_0(E)$ remains as either 0 or 1 as the temperature changes, so that $\frac{\partial f_0(E)}{\partial T}$ is non-zero only when E is close to μ. Therefore, equation (92) can be approximated by taking $v = v_F$ and $\tau = \tau_F$, i.e. the Fermi velocity and the scattering mean free time of Fermi electrons;

$$k_e = \frac{1}{3}{v_F}^2\tau_F \int_{E=0}^{\infty} \frac{\partial f_0(E)}{\partial T} D(E)(E-\mu)dE = \frac{1}{3}{v_F}^2\tau_F C_e = \frac{1}{3}C_e v_F l_F \qquad (93)$$

This is essentially the Kinetic theory expression of thermal conductivity.

Wiedemann–Franz law

From equation (63), the electrical conductivity is;

$$\sigma \equiv \frac{J_z}{E_z} = -\frac{2e^2}{3m}\int_{E=0}^{\infty}\frac{\partial f_0}{\partial E}D(E)E\tau dE \tag{93}$$

$\frac{\partial f_0(E)}{\partial E}$ is non–zero only when E is close to μ, and can be approximated to as a delta function

$$\frac{\partial f_0(E)}{\partial E} \approx -\delta(E-\mu) \tag{94}$$

Combining equation (94) and (93) gives;

$$\begin{aligned}\sigma \equiv \frac{J_z}{E_z} &= \frac{2e^2}{3m}\int_{E=0}^{\infty}\delta(E-\mu)D(E)E\tau dE \\ &= \frac{2e^2}{3m}D_{E=\mu}\mu\tau_{E=\mu} = \frac{2e^2}{3m}D_F\mu\tau_F\end{aligned} \tag{95}$$

Using $\mu \approx E_F = mv_F{}^2/2$ reduces equation (95) to

$$\sigma = \frac{e^2}{3}D_F v_F{}^2\tau_F \tag{96}$$

Note that, the electron concentration can be calculated as;

$$\begin{aligned}n &= \int_{E=0}^{\infty} f_0(E)D(E)dE = \int_{E=0}^{\infty} f_0(E,T=0)D(E)dE = \int_{E=0}^{E_F} D(E)dE \\ &= \int_{E=0}^{E_F}\frac{1}{2\pi^2}\left(\frac{2m}{\hbar^2}\right)^{2/3}E^{1/2}dE = \frac{1}{3\pi^2}\left(\frac{2m}{\hbar^2}\right)^{2/3}E_F{}^{3/2} = \frac{2}{3}D_F E_F \approx \frac{2}{3}D_F\mu\end{aligned} \tag{97}$$

Combining equation (97) and (95) gives;

$$\sigma = \frac{e^2}{m}n\tau_F \tag{98}$$

Use the following definition of electron mobility;

$$\mu_e = \frac{e}{m}\tau_F \tag{99}$$

From equation (97)

$$\sigma = ne\mu_e \tag{100}$$

Note that, μ_e is electron mobility and is different from μ which is chemical potential. Equation (98) and (92) can be used to calculate the ratio between the electron thermal conductivity and electrical conductivity.

$$\frac{k_e}{\sigma} = \frac{\frac{1}{3}v_F{}^2\tau_F C_e}{\frac{e^2}{m}n\tau_F} = \frac{mC_e v_F{}^2}{3ne^2} \tag{101}$$

Here it is assumed that the τ_F is the same in the thermal conductivity and electrical conductivity expressions. These two τ_F terms can be different.

Note that, the electron specific heat of metals has been derived previously as

$$C_e = \frac{1}{2}\pi^2 nk_B T / T_F = \frac{\frac{1}{2}\pi^2 nk_B T}{\frac{mv_F{}^2}{2k_B}} = \frac{\pi^2 nk_B^2 T}{mv_F{}^2} \tag{102}$$

Combining equation (101) and (102) gives;

$$\frac{k_e}{\sigma} = \frac{mv_F{}^2}{3ne^2}\frac{\pi^2 nk_B^2 T}{mv_F{}^2} = \frac{\pi^2 k_B^2 T}{3e^2} \tag{103}$$

The Lorentz number is defined as;

$$L = \frac{\pi^2 k_B^2}{3e^2} = 2.45 \text{ x } 10^{-8}(\text{W}\Omega\ \text{K}^{-2}) \tag{104}$$

So that the Wiedemann–Franz law is;

$$\frac{k_e}{\sigma} = LT \tag{105}$$

Electrical conductivity

Combining equation (63), (67) and (68) gives;

$$\sigma = -\frac{2q^2}{3m}\int_{E=0}^{\infty}\frac{\partial f_0}{\partial E}\frac{(2m)^{3/2}}{2\pi^2\hbar^3}E^{1/2}\cdot E^r\cdot EdE$$
$$= -\frac{q^2}{3m}\frac{(2m)^{3/2}}{\pi^2\hbar^3}\int_{E=0}^{\infty}\frac{\partial f_0}{\partial E}E^{r+3/2}dE \qquad (106)$$

The integral in equation (105) can be simplified using the product rule in equation (70);

$$\sigma = -\frac{q^2}{3m}\frac{(2m)^{3/2}}{\pi^2\hbar^3}\left(r+\frac{3}{2}\right)\int_{E=0}^{\infty}f_0E^{r+1/2}dE \qquad (107)$$

Equation (107) uses the Fermi–Dirac integral in equation (72) and (73);

$$\sigma = -\frac{q^2}{3m}\frac{(2m)^{3/2}}{\pi^2\hbar^3}\left(r+\frac{3}{2}\right)(k_{\mathrm{B}}T)^{r+3/2}F_{r+1/2}(\eta) \qquad (108)$$

Electrical conductivity for metals

For metals with $\eta = \mu/k_{\mathrm{B}}T >> 0$, the Fermi–Dirac integral can be expressed in the form of a rapidly converging series as shown for equation (75);

$$\sigma = -\frac{q^2}{3m}\frac{(2m)^{3/2}}{\pi^2\hbar^3}\left(r+\frac{3}{2}\right)(k_{\mathrm{B}}T)^{r+3/2}\left(\frac{\eta^{r+3/2}}{(r+3/2)}+(r+1/2)\eta^{r-1/2}\frac{\pi^2}{6}\right)$$
$$= -\frac{q^2}{3m}\frac{(2m)^{3/2}}{\pi^2\hbar^3}\left(r+\frac{3}{2}\right)(k_{\mathrm{B}}T)^{r+3/2}\frac{\eta^{r+3/2}}{(r+3/2)}+\frac{q^2}{3m}\frac{(2m)^{3/2}}{\pi^2\hbar^3}\left(r+\frac{3}{2}\right)(k_{\mathrm{B}}T)^{r+3/2}\left(r+\frac{1}{2}\right)\eta^{r-1/2}\frac{\pi^2}{6}$$
$$= -\frac{q^2}{3m}\frac{(2m)^{3/2}}{\pi^2\hbar^3}(k_{\mathrm{B}}T)^{r+3/2}\eta^{r+3/2}+\frac{q^2}{3m}\frac{(2m)^{3/2}}{\pi^2\hbar^3}\left(r+\frac{3}{2}\right)(k_{\mathrm{B}}T)^{r+3/2}\left(r+\frac{1}{2}\right)\eta^{r-1/2}\frac{\pi^2}{6}$$
$$= -\frac{q^2}{3m}\frac{(2m)^{3/2}}{\pi^2\hbar^3}(k_{\mathrm{B}}T)^{r+3/2}\left(\frac{\mu}{k_{\mathrm{B}}T}\right)^{r+3/2}+\frac{q^2}{3m}\frac{(2m)^{3/2}}{\pi^2\hbar^3}\left(r+\frac{3}{2}\right)(k_{\mathrm{B}}T)^{r+3/2}\left(r+\frac{1}{2}\right)\left(\frac{\mu}{k_{\mathrm{B}}T}\right)^{r-1/2}\frac{\pi^2}{6}$$
$$= -\frac{q^2}{3m}\frac{(2m)^{3/2}}{\pi^2\hbar^3}\mu^{r+3/2}+\frac{q^2}{3m}\frac{(2m)^{3/2}}{\pi^2\hbar^3}\left(r^2+2r+\frac{3}{4}\right)(k_{\mathrm{B}}T)^2\mu^{r-1/2}\frac{\pi^2}{6}$$
$$= -\frac{q^2}{3m}\frac{(2m)^{3/2}}{\pi^2\hbar^3}\left(\mu^{r+3/2}+\frac{\pi^2}{6}(k_{\mathrm{B}}T)^2\left(r^2+2r+\frac{3}{4}\right)\mu^{r-1/2}\right) \qquad (109)$$

where μ is chemical potential, assuming $\mu \approx E_F$. Taking $q = -e$ and $\mu = E_{\mathrm{F}}$ in equation (109);

$$\sigma_{\mathrm{metal}} = \frac{e^2}{3m}\frac{(2m)^{3/2}}{\pi^2\hbar^3}\left((E_{\mathrm{F}})^{r+3/2} + \frac{\pi^2}{6}(k_{\mathrm{B}}T)^2\left(r^2 + 2r + \frac{3}{4}\right)(E_{\mathrm{F}})^{r-1/2}\right) \qquad (110)$$

Electrical conductivity for semiconductors

For semiconductors $\frac{E-\mu}{k_{\mathrm{B}}T} = \zeta - \eta > 3$ using the Fermi–Dirac integrals from equations (76) and (78) in equation (107);

$$\begin{aligned}\sigma &= -\frac{q^2}{3m}\frac{(2m)^{3/2}}{\pi^2\hbar^3}\left(r+\frac{3}{2}\right)(k_{\mathrm{B}}T)^{r+3/2}\exp(\eta)\Gamma(r+5/2) \\ &= -\frac{q^2}{3m}\frac{(2m)^{3/2}}{\pi^2\hbar^3}k_{\mathrm{B}}T\left(r+\frac{3}{2}\right)\exp(\eta)\left(r+\frac{3}{2}\right) \\ &= -\frac{2q^2}{3m}\frac{(2m)^{3/2}}{\pi^2\hbar^3}k_{\mathrm{B}}T\left(r+\frac{3}{2}\right)\exp\left(\frac{\mu}{k_{\mathrm{B}}T}\right)\end{aligned} \qquad (111)$$

Take $q = -e$ and $\mu = E_{\mathrm{F}}$ in equation (111);

$$\sigma_{\mathrm{semi}} = \frac{2e^2}{3m}\frac{(2m)^{3/2}}{\pi^2\hbar^3}k_{\mathrm{B}}T\left(r+\frac{3}{2}\right)\exp\left(\frac{E_{\mathrm{F}}}{k_{\mathrm{B}}T}\right) \qquad (112)$$

Molecular dynamics

Molecular dynamics method

Molecular dynamics (MD) is a computer simulation technique that allows one to predict the time evolution of a system of interacting particles (atoms, molecules, granules, etc.). The basic idea is simple. First, for a system of interest, one has to specify a set of initial conditions (initial positions & velocities of all particles in the system) and interaction potential for deriving the forces among all the particles. Second, the evolution of the system in time can be followed by solving a set of classical equations of motion for all particles in the system. Within the framework of

classical mechanics, the equations that govern the motion of classical particles are the ones that correspond to the second law of classical mechanics formulated by Sir Isaac Newton;

$$\vec{F}_i = m_i \vec{a}_i = m_i \frac{\partial \vec{v}_i}{\partial t} = m_i \frac{\partial^2 \vec{r}_i}{\partial t^2} \tag{113}$$

where F , m , r , v and a are force, mass, position, velocity and acceleration for the i^{th} particle, t is time. If the particles of interest are atoms, and if there are a total of N of them in the system, the force acting on the i^{th} atom at a given time can be obtained from the interatomic potential $U(\vec{r}_1, \vec{r}_2, \vec{r}_3, , \ldots, \vec{r}_N)$ that, in general, is a function of the positions of all the atoms;

$$\vec{F}_i = -\vec{\nabla} U_i(\vec{r}_1, \vec{r}_2, \vec{r}_3, , \ldots, \vec{r}_N) \tag{114}$$

Once the initial conditions and the interaction potential are defined, the equations of motion can be solved numerically. The results of the solution are the positions and velocities of all the atoms as a function of time, $\vec{r}_i(t)$, $\vec{v}_i(t)$. The solution of the MD method can be obtain by solving equation (113) and (114).

Thus;

$$E_i = U_{ij} + E_{Ki} = U_{ij} + \frac{1}{2} m_i v_i^2 \tag{115}$$

where E_i is total energy for the i^{th} particle, obtained by the sum of energy in the system and E_{Ki} is the kinetic energy for the i^{th} particle.

Pair potentials

The total potential energy of the system of N atoms interacting via pair potential is:

$$U(\vec{r}_1, \vec{r}_2, \vec{r}_3, , \ldots, \vec{r}_N) = \sum_i \sum_{j>i} U_2(r_{ij}); \quad r_{ij} = \left| \vec{r}_j - \vec{r}_i \right| \tag{116}$$

Commonly used examples of pair potentials are;

Hard/soft spheres – the simplest potential without any cohesive interaction. Useful in theoretical investigations of some idealized problems.

hard;

$$U(r_{ij}) = \begin{cases} \infty & \text{for} \quad r_{ij} \le r_0 \\ 0 & \text{for} \quad r_{ij} > r_0 \end{cases} \tag{117}$$

soft;

$$U(r_{ij}) = \left(\frac{r_{ij}}{r_0} \right)^{-n} \tag{118}$$

Ionic – Coulomb interaction of charges (q), strong, long range repulsion or attraction; often added to other functional forms to account for charge–charge interaction or polarization.

$$U(r_{ij}) = \frac{q_i q_j}{r_{ij}} \tag{119}$$

Lennard–Jones – van der Waals interaction in inert gases and molecular systems. Often used to model general effects rather than properties of a specific material (Lennard–Jones, 1924, pp.463–477).

$$U(r_{ij}) = 4\varepsilon \left(\left(\frac{\sigma}{r_{ij}} \right)^{12} - \left(\frac{\sigma}{r_{ij}} \right)^{6} \right) \tag{120}$$

where ε and σ are depth of the potential well and the finite distance at which the inter–particle potential is zero, respectively.

Morse – similar to Lennard–Jones but is a more "bonding–type" potential and is more suitable for cases where attractive interaction comes from the formation of a chemical bond. Proposed by Morse (1929, pp.57–65). It was a popular potential for the simulation of metals that have fcc and hcp structures. A fit for many metals is given by Girifalco and Weizer (1959, pp.687–690).

$$U(r_{ij}) = \varepsilon\left(\mathrm{e}^{-2\alpha\left(r_{ij}-r_0\right)} - 2\,\mathrm{e}^{-\alpha\left(r_{ij}-r_0\right)}\right) \tag{121}$$

where α is the shape of the potential well.

6-exponential Buckingham (1938, pp.264-283) potential-exponential term (Born-Mayer) provides a better description of strong repulsion due to the overlap of the closed shell electron clouds, which is important in the simulation of bombardment by energetic atoms or ions, etc.;

$$U(r_{ij}) = A\,\mathrm{e}^{-r_{ij}/R_{\mathrm{BM}}} - B / r_{ij}^{6} \tag{122}$$

where R_{BM} is the distance of Born-Mayer.

One can assume a functional form for the potential function and then choose the parameters to reproduce a set of experimental data. This gives so-called "empirical potential functions". The choice of a potential function that approximates the actual (unknown) solution is a difficult task. Design of the potential function and choice of the parameters is often based on its fit with the experimental data that is available, (e.g. equilibrium geometry of stable phases, cohesive energy, elastic moduli, vibrational frequencies, temperatures of the phase transitions, etc.).

Green-Kubo relation

Simply stated, the Green-Kubo relation for bulk viscosity (Zwanzig, 1965, pp.67-102) is,

$$\eta_V = \frac{1}{Vk_{\mathrm{B}}T}\int_0^{\infty} \mathrm{d}t \left\langle \left(p(t)V(t) - \langle pV \rangle \right)\left(p(0)V(0) - \langle pV \rangle \right) \right\rangle \tag{123}$$

The Green-Kubo relation for thermal conductivity can be derived by similar arguments to those used in the viscosity derivation.

Firstly, for the velocity gradient, the internal energy per unit volume ρU obeys a continuity equation, $\rho \mathrm{d}U / \mathrm{d}t = -\nabla J_{\mathrm{Q}}$. Secondly, we note that Fourier's definition of the thermal conductivity coefficient κ, is $J_{\mathrm{Q}} = -\kappa \nabla T$. Combining these two results we obtain

$$\rho \frac{\mathrm{d}U}{\mathrm{d}t} = \lambda \nabla^2 T \tag{124}$$

Unlike the previous examples, both U and T have nonzero equilibrium values; namely, $\langle U \rangle$ and $\langle T \rangle$. A small change in the left-hand side of the equation (2.5.11) can be written as $(\rho + \Delta\rho)\frac{\mathrm{d}\langle U \rangle + \Delta U}{\mathrm{d}t}$. By definition $\frac{\mathrm{d}\langle U \rangle}{\mathrm{d}t} = 0$, so for the first order in Δ, we have $\rho \frac{\mathrm{d}U}{\mathrm{d}t} = 0$. Similarly, the spatial gradient of $\langle T \rangle$ does not contribute, so it can be written as;

$$\rho \frac{\mathrm{d}U}{\mathrm{d}t} = \lambda \nabla^2 \Delta T \tag{125}$$

The next step is to relate the variation in temperature ΔT to the variation in energy per unit volume $\Delta(\rho U)$. To do this we use the thermodynamic definition;

$$\frac{1}{V}\frac{\partial E}{\partial T}\bigg|_V = \frac{\partial(\rho U)}{\partial T}\bigg|_V = \rho C_V \tag{126}$$

where C_V is the heat capacity at constant volume. We see from the second equality, that a small variation in the temperature ΔT is equal to $\Delta(\rho U) / \rho C_V$. Therefore;

$$\rho \Delta U = \frac{\kappa}{\rho C_V} \nabla^2 \rho \Delta U \tag{127}$$

If $D_T \equiv \kappa / \rho C_V$ is the thermal diffusivity, then in terms of the wavevector, the dependent internal energy density equation (127) becomes;

$$\rho \Delta U(\mathrm{k}, t) = -\mathrm{k}^2 D_T \rho \Delta U(\mathrm{k}, t) \tag{128}$$

If $C(\mathrm{k},t)$ is the wavevector dependent internal energy density autocorrelation function,

$$C(\mathrm{k},t)=\left\langle \rho\Delta U(\mathrm{k},t)\rho\Delta U(-\mathrm{k},0)\right\rangle \tag{129}$$

Then the frequency and wavevector dependent diffusivity is the memory function of the energy density autocorrelation function;

$$\tilde{C}(\mathrm{k},\omega)=\frac{C(\mathrm{k},0)}{i\omega+\mathrm{k}^2\tilde{D}_T(\mathrm{k},\omega)} \tag{130}$$

Equation (130) can be converted to an expression for the diffusivity in terms of a current correlation function. From the flux autocorrelation function $\phi(t)$ as shown equation (131) and (132).

$$\phi(t)=\left\langle A(t)A^*(0)\right\rangle \tag{131}$$

$$-\tilde{\phi}(s)=\int_0^\infty \mathrm{d}t\mathrm{e}^{-st}\frac{\mathrm{d}^2C(t)}{\mathrm{d}t^2}=\left[\mathrm{e}^{-st}\frac{\mathrm{d}C(t)}{\mathrm{d}t}\right]_0^\infty+s\int_0^\infty \mathrm{d}t\mathrm{e}^{-st}\frac{\mathrm{d}C(t)}{\mathrm{d}t}$$

$$=s\left[\mathrm{e}^{-st}C(t)\right]_0^\infty+s^2\int_0^\infty \mathrm{d}t\mathrm{e}^{-st}C(t)=s^2\tilde{C}(s)-sC(0) \tag{132}$$

if $\phi=-\mathrm{d}^2C/\mathrm{d}t^2$ then,

$$\phi(\mathrm{k},t)=\mathrm{k}^2\left\langle J_{\mathrm{Q}x}(\mathrm{k},t)J_{\mathrm{Q}x}(-\mathrm{k},0)\right\rangle \tag{133}$$

Using equation (132), the analogue is obtained;

$$\tilde{K}(s)=\frac{\tilde{\phi}(s)}{C(0)-\dfrac{\tilde{\phi}(s)}{s}} \tag{134}$$

$$\mathrm{k}^2D_T(\mathrm{k},\omega)=\frac{C(\mathrm{k},0)-i\omega\tilde{C}(\mathrm{k},\omega)}{\tilde{C}(\mathrm{k},\omega)}=\frac{\tilde{\phi}(\mathrm{k},\omega)}{C(\mathrm{k},0)-\dfrac{\tilde{\phi}(\mathrm{k},\omega)}{i\omega}} \tag{135}$$

$$N(\mathrm{k},t)\equiv\frac{1}{Vk_{\mathrm{B}}T}\left\langle P_{yx}(\mathrm{k},t)P_{yx}(-\mathrm{k},0)\right\rangle \tag{136}$$

By defining the analogue of equation (136) (called the autocorrelation function of the wavevector dependent shear stress), that is $\phi(\mathrm{k},t)=\mathrm{k}^2 N_{\mathrm{Q}}(\mathrm{k},t)$, equation (135) for the thermal diffusivity can be written in the same form as the wavevector dependent shear viscosity. That is;

$$\tilde{D}_T(\mathrm{k},\omega)=\frac{\tilde{N}_{\mathrm{Q}}(\mathrm{k},\omega)}{C(\mathrm{k},0)-\dfrac{\mathrm{k}^2}{i\omega}\tilde{N}_{\mathrm{Q}}(\mathrm{k},\omega)} \tag{137}$$

Note that, the zero wavevector limit must be taken before the zero frequency limit is taken, and the canonical ensemble fluctuation formula is used for the specific heat;

$$\rho C_V=\frac{C(0,0)}{Vk_{\mathrm{B}}T^2} \tag{138}$$

The Green–Kubo expression for the thermal conductivity is obtained as;

$$\kappa=\frac{V}{k_{\mathrm{B}}T^2}\int_0^\infty \mathrm{d}t\left\langle J_{\mathrm{Q}x}(t)J_{\mathrm{Q}x}(0)\right\rangle \tag{139}$$

(Sarman & Evans, 1993, pp.9021–9036)

Carbon nanotubes

Carbon nanotubes (CNTs) are a tubular form of carbon with an exceptionally high aspect ratio, located structurally between planar graphene/graphite layers and molecular fullerenes. Their electrical properties have initiated a tremendous number of theoretical and experimental studies. This has been supported by progress in the micro–fabrication processes of metals and semiconductors, which has opened the way to electrical contacting of single molecules or a relatively small number of molecules. This and the potential use of CNTs for organic based integrated circuits as conducting wires on a molecular scale, as well as being an electrically active element itself, whilst

also being an almost perfect model system for fundamental research, justifies the fascination of this molecular based structure (Loiseau, Launois, Petit, Roche & Salvetat, 2006; Reich, Thomsen & Maultzsch, 2004).

A single walled carbon nanotube (SWNT) is structurally equivalent to a sheet of graphene rolled into a tube (see Figure 5), i.e. each carbon atom has three neighbors, lying in the plane of the tube wall in a hexagonal arrangement. Such an arrangement minimizes the number of carbon dangling bonds since it has no edge sites compared to an equivalent graphene sheet. Energetically offset against this is the out–of–plane distortion caused by the curvature of the tube wall.

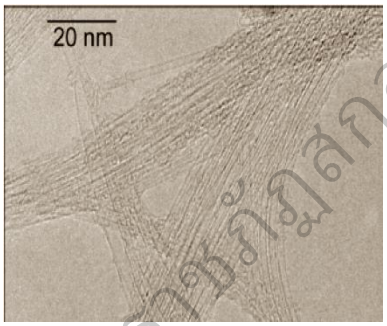

Figure 5 Single walled nanotubes arranged in bundles (SWNT)

Multi–walled nanotubes (MWNTs) consist of multiple tubes arranged coaxially, with a typical inter–wall spacing of 0.34–0.36 nm, reminiscent of turbostratic graphite (see Figure 6). In principle MWNTs span the whole gamut from double walled nanotubes (DWNTs) – having diameters close to those of SWNTs – up to macroscopic carbon fibers, which have been shown to sometimes feature nanotubes at their cores. Obviously a material spanning such a wide range of dimensions from nano to microscopic can have a similarly varying range of properties. What is commonly referred to as a MWNT typically has a diameter much greater than that of SWNTs, with the number of concentric walls varying from two up to several hundreds.

Figure 6 Multi–walled nanotube (MWNT) tube wall

Physical structure of carbon nanotubes

A carbon nanotube can be obtained by rolling up the graphene sheet seamlessly along a certain direction. For this it is very importan to define at least two lattice sites which have to be included the overlap. All of the others are then sites are determined by the six–fold symmetry of the graphene lattice and the cylindrical configuration of the CNT. These two initial points can be connected by the chiral vector;

$$\vec{C}_{n,m} = n\vec{a}_1 + m\vec{a}_2 \qquad (140)$$

This is just a linear combination of $\vec{a}_1$ and $\vec{a}_2$ where n , m are integers. The symmetry of the graphite lattice is such that chiral vectors with $m > n$ have symmetric equivalents with $m < n$, so therefore condition is imposed that $m \geq n$. Thus a particular SWNT can be defined using a pair of integer indices (n, m), which together define the chiral vector of the nanotube, as shown in Figure 7.

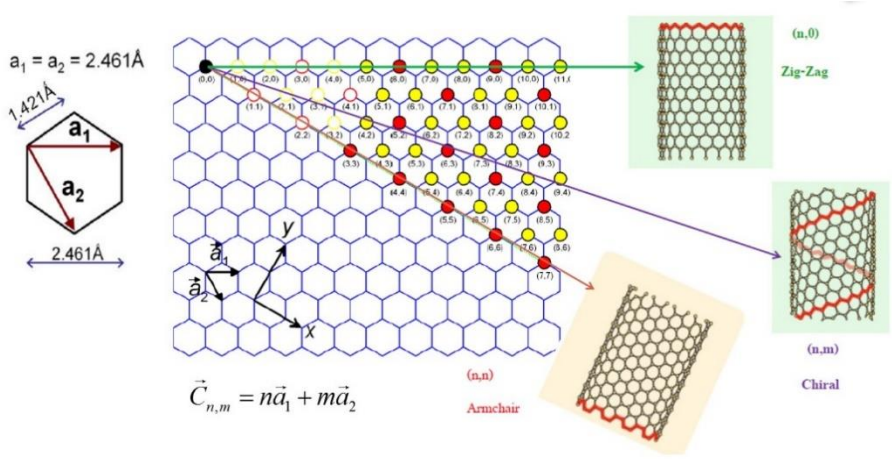

Figure 7 Graphene sheet showing the sixfold–symmetry (left) and chiral vector

Due to the sixfold symmetry of the graphene lattice, all possible structures can be classified by three general configurations: armchair CNTs, for which $n = m$, zigzag CNTs that have $n = 0$ and all other CNTs which are referred to as chiral, as shown in Figure 8. This use of the term chiral is to some extent misleading (indeed, helical is more appropriate). Often armchair and zigzag nanotubes are also called chiral, although their mirror images are identical to the original.

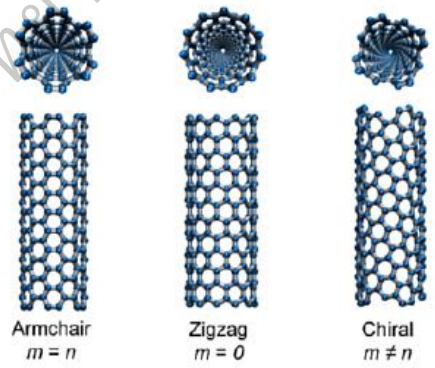

Figure 8 The three types of CNTs viz. armchair chiral and zig–zag (Johnson, & Kohlmeyer, About Carbon / Boron Nitride Nanostructure Builder Plugin, http://www.ks.uiuc.edu/Research/vmd/plugins/nanotube, 4 January 2016)

Electronic structure of carbon nanotubes

The electronic properties of the graphene sheet (and thus of the CNTs) are mainly determined by the π –electrons, since the electrons in the sp^2–hybridised orbitals are strongly localized. In particular, the interaction between the p_z–orbitals leads to (i) the delocalization of the π –electrons and (ii) the formation of bonding π –bands and antibonding π^* –bands.

For CNTs, periodic boundary conditions are introduced to the planar two–dimensional graphene–sheet model due to the translational symmetry around the circumference of the CNT. To discuss this further it is convenient to shift our focus to reciprocal space. The reciprocal lattice of a graphene layer is again a honeycomb–lattice. A three–dimensional graph of the energy dispersion of graphene of the two lowest sub–bands in the first BZ, is given in Figure 9 (left), derived by tight binding calculations (Saito, Dresselhaus & Dresselhaus, 1998). The six points denoted by K at the edge of the BZ are the only points where the π – and π^* –band touch, and are the reason graphene is a semi–metal. Seen in projection this gives a hexagonal reduced BZ, with the K –points located at the hexagonal corners as show in Figure 9(right).

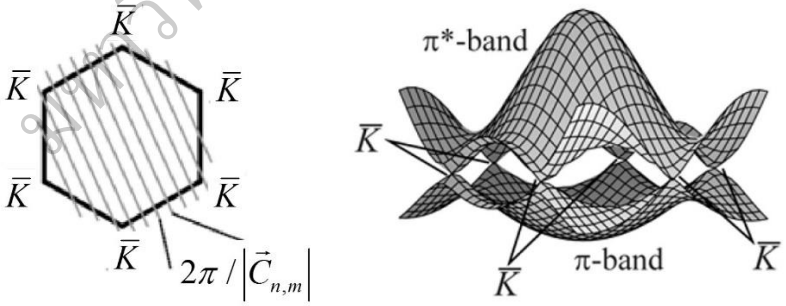

Figure 9 2D graphene showing six points denoted by K at the edge of the BZ (left) π – and π^* –band from a tight–binding calculation of CNTs (right)

It is then clear that the band gap of the nanotube will be determined by the position of these lines on the 2D graphene BZ. Slices which cross the K –points

are describing metallic CNTs, as at these points the π – and π^* energy band touch. This in turn leads to a finite density of states at the Fermi energy E_F. Other directions correspond to CNTs with a vanishing DOS at E_F, resulting in an energy–gap of typically less than 1 eV. These CNTs are therefore semiconducting.

The information needed to decide whether a CNT is metallic or semiconducting can be again extracted from the integers (n,m) that classify each CNT, as described above. The pair of indices (n,m) defines the basic electronic character of the nanotube, If $n=m$ and if $nm=3i$ (where i =integer, $i\neq 0$) the tube is semi–metallic otherwise it is semiconducting. All armchair tubes are metallic whereas zigzag and chiral nanotubes can exist as either metallic or semiconducting molecular structures, as shown in Figure 10.

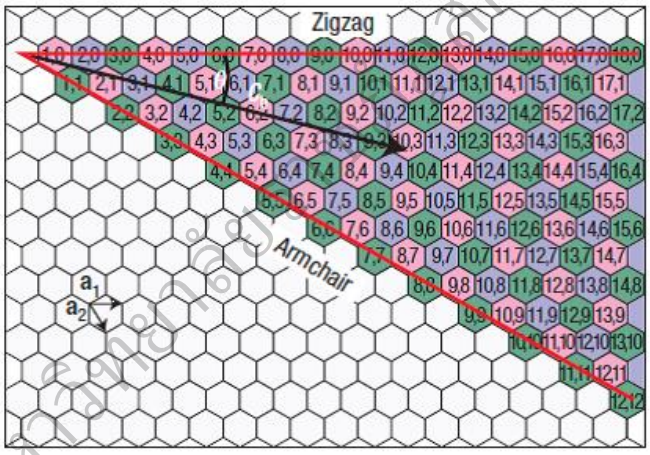

Figure 10 Periodic table of carbon nanotubes (Aliofkhazraei, 2015)

Since all of the above discussion of the electronic properties of isolated SWNTs is based around a graphene model, we would expect deviations from this due to the effects of curvature on the bonding in the nanotube. For example, C–C bond lengths become slightly polarized; axially oriented bonds shorten and circumferential bonds elongate by a few fractions of a percent depending on curvature, as curvature weakens the non–axial π–bonding and consequent aromaticity. This may have a weak effect on conduction pathways and bond site reactivity.

Thermoelectric power of carbon nanotubes

The thermoelectric power of early samples, consisting of mats, bundles, and multiwalls, showed a large thermopower. Values were as high as 80 μV K^{-1} (Mahan & Jeon, 2004, p. 075405) at room temperature. The variations with in temperature, from low to high temperature (T = 300 K), were not linear but had a hump, as shown in Figure 11 (left). This hump was attributed to phonon–drag, (Romero, Sumanasekera, Mahan, & Eklund, 2002, p. 205410) about which there are several theoretical papers. (Scarola, & Mahan, 2002, p. 205405; Vavro et al., 2003, p. 065503). However, we now think these theories are all incorrect, even those of the author. A carbon nanotube without defects can either be metallic or semiconducting. Most researchers expect that the high value of the Seebeck coefficient is found in semiconductor tubes, since metallic systems usually have a smaller value for the Seebeck. Carbon nanotubes have electron–hole symmetry and the energy bands look the same if you rotate them upside down. The transport of holes is identical to the transport of electrons. They cancel out, so there is no thermopower. This argument is rigorous if the tube is undoped, so the chemical potential is at the point where the conducting bands cross in metallic tubes. The usual theory of phonon–drag makes the following assumptions:

(i) The electron–phonon interaction can cause the thermopower. This assumption is incorrect, since the hole–phonon interaction is identical to that of the electron–phonon. The interaction with phonons does not break electron–hole symmetry, and the thermopower is still zero.

(ii) Doping the nanotube moves the chemical potential away from the point where there are equal numbers of electrons and holes. However, a small amount of doping moves the chemical potential a small amount, and in this region one can still find that the transport density of states $D(\mu)$ is a constant. According to the Mott relation;

$$S = \frac{\pi^2}{3}\frac{k_B^2 T}{e}\frac{\mathrm{d}}{\mathrm{d}\mu}\ln\left[D(\mu)\right] \tag{141}$$

$S = 0$ if $\mathrm{d}D(\mu)/\mathrm{d}\mu = 0$; which it does in a metallic tube, where μ is the chemical potential.

(iii) The phonon–drag effect only contributes to the thermopower when impurities break electron–hole symmetry. Kostyrko (Kostyrko, Bartkowiak, & Mahan, 1999a, p. 3241; Kostyrko, Bartkowiak, & Mahan, 1999b, p. 10735) calculated the density of states for a metallic (10,10) armchair tube, which contained about 1% nitrogen impurities. The density of states is shown in Figure 11(right) as the dashed line. The solid line in the Figure is the density of states without impurities, which is indeed constant near the zero of energy.

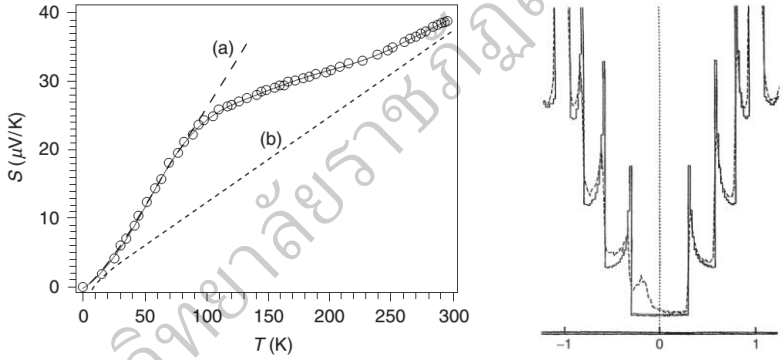

Figure 11 Seebeck coefficient versus temperature (right) and density of state of a (10,10) CNTs with 1% nitrogen impurity (right)

The nitrogen impurities cause the resonance in the density of states to move close near to zero energy. Mahan showed it was actually a resonance associated with the semiconductor band that was higher in energy. (Mahan, 2004, p. 125407) This resonance structure gives rise to a nonzero Seebeck coefficient, and accounts for the large values observed in the early experiments. The early measurements of the Seebeck found large values caused by band resonances from impurity states.

Literature reviews

I will review the history of Calcium Manganese Oxide in the field of thermoelectric research, as well as the development of thermoelectric properties.

Generally, a Calcium Manganese Oxide ($CaMnO_3$) compound is an *n*–type thermoelectric material. $CaMnO_3$ has two lattice structures. One lattice is the Perovskite structure (space group number: 221, space group symbol: *Pm–3m*) with lattice parameters a = b = c = 7.46 Å. The other lattice is the orthorhombic structure (space group number: 62, space group symbol: *Pnma*) with lattice parameters a =5.2812 Å, b = 5.2753 Å and c = 7.48 Å.

Ansell (Ansell, Modrick, Longo, Poeppelmeier, & Horowitz, 1982, pp.1795–1797) reported that $Ca_2Mn_3O_8$ has a monoclinic structure with space group symbol C2/m, lattice parameter a=11.0144 Å, b =5.8513 Å, c=4.92422 Å, angle β =109.735° and density 4.13 g cm^{-3}. This is the first reported example of a compound possessing pragmatically coordinated Ca^{2+} ions. They separate $Mn_3(O_8)^{4-}$ sheets formed by the edgs–sharing of distorted MnO_6 octahedra.

Reller (Reller, Jefferson, Thomas & Uppal, 1983, pp.913–914) studied $CaMnO_{2.8}$ by a high–resolution electron microscopy technique and computer simulation. He reported that nonstoichiometric phase $CaMnO_{2.8}$ is made up of ordered intergrowths of corner–shared MnO_8 octahedral and MnO_5 square pyramids, with a new structure having been formed form the parent ideal cubic structure $CaMnO_3$ (a=b=c= 3.73 Å) via regular removal of O^{2-}.

Ohtaki (Ohtaki et al., 1995, pp.105–111) prepared $(Ca_{0.9}M_{0.1})MnO_3$ (M = Y, La, Ce, Sm, In, Sn, Sb, Pb, Bi) by the solid state reaction (SSR) method. They reported that the substitution at the Ca site increased the electrical conductivity, along with a moderate decrease in the absolute value of the Seebeck coefficient. $(Ca_{0.9}Bi_{0.1})MnO_3$ exhibits the largest power factor, 2.8×10^{-4} W m^{-1} K^{-2} at 1000 K^{-1} and shows ZT 0.085 at 1173 K.

Zeng (Zeng, Greenblatt & Croft, 1999, pp.8784–8788) prepared $CaMnO_{3-\delta}$ by the sol–gel method at 1373 K. They reported that the valence of Mn in $CaMnO_3$ is close to 4+ and Mn^{3+} is created by two Mn^{3+} five coordinate sites for each O vacancy. The valence of Mn exhibits +3.88, +3.78 at $O_{2.94}$ and $O_{2.89}$ respectively. With decreased oxygen content, its affect is to increase the unit cell volume.

Xu (Xu et al., 2004, pp.147–151) prepared $CaMn_{1-X}M_XO_3$ (M = Nb and Ta; $0 \leq X \leq 0.3$) by the SSR method. They reported that the lattice parameters a and b increased, whereas c decreased with Na– and Ta–doped. Furthermore, Nb^{5+} and Ta^{5+} have an ion radius greater than Mn^{4+} which causes the tetragonal structure to change to an orthorhombic structure. The electrical resistivity and absolute Seebeck coefficient both decreased by virtue of Na– and Ta–doped. Overall a good thermoelectric performance was displayed, with the Figure of merit $Z = 0.8\times10^{-4}$ W m^{-1} K^{-2} at 1000 K for $CaMn_{0.96}Nb_{0.04}O_3$ and $Z = 0.5\times10^{-4}$ W m^{-1} K^{-2} at 1000 K for $CaMn_{0.96}Ta_{0.04}O_3$.

Zhou (Zhou & Kennedy, 2006, pp.1595–1598) prepared $CaMnO_3$ by the SSR method and studied the expansion of its orthorhombic structure using a high–resolution synchrotron X–ray diffraction technique, at room temperature through to 1073 K. They reported that the bond length of Mn–O(1) = 1.8972 Å, Mn–O(2) = 1.8982 Å, and 1.9072 Å increased to 1.9061 Å, 1.9075 Å and 1.9115 Å, respectively. The lattice parameter a=5.2674 Å, b=5.2828 Å, c=7.5457 Å increased to a=5.3181 Å, b=5.3125 Å, c=7.5254 Å as non–phases change.

Yamashita (Yamashita, 2007, pp.461–464) prepared $Ca_{1-X}Na_XMnO_3$ ($0 \leq x \leq 0.025$) by the SSR method. He reported that the hole carriers may be doped in $Ca_{0.99}Na_{0.01}MnO_3$ which has the lowest resistivity and smallest band gap. The electrical resistivity's are $\rho(Ca_{0.99}Na_{0.01}MnO_3) < \rho(Ca_{0.98}Na_{0.02}MnO_3) < \rho(Ca_{0.975}Na_{0.025}MnO_3) < \rho(CaMnO_3)$ which indicated Na did not increase the carrier concentration, which agrees with a band gap of 0.39 eV for $CaMnO_3$, 0.11 eV for $Ca_{0.99}Na_{0.01}MnO_3$, 0.145 eV for $Ca_{0.98}Na_{0.02}MnO_3$, and 0.275 eV for $Ca_{0.975}Na_{0.025}MnO_3$.

Sousa (Sousa, et al., 2008, pp.311–319) prepared $Ca_{1-X}Ho_XMnO_3$ ($0.1 \leq X \leq 0.4$) by the citrate–nitrate sol–gel route method. They reported that $Ca_{1-X}Ho_XMnO_3$ has a Perovskite orthorhombic (*Pnma*) structure at $0 \leq X \leq 0.2$ and a monoclinic ($P2_1/m$) structure at $0.3 \leq X \leq 0.4$. The small Ho concentration produces an important decrease in the electrical resistivity and induces an electrical transition.

Lan (Lan et al., 2009, pp.535–538) prepared $Ca_{1-X}La_XMnO_3$ (X = 0, 0.02, 0.04, 0.06, 0.08) by the SSR method. They reported that $Ca_{1-X}La_XMnO_3$ has a Perovskite orthorhombic and the unit cell increased with increasing La. It's affect was to enhance the power factor.

Park (Park, Kwak & Yoon, 2009, pp.550–555) prepared $Ca_{1-x}Bi_xMn_{1-y}NbyO_3$ ($0 \leq x=y \leq 0.1$) by the SSR method. They reported that the lattice parameter of the orthorhombic increased with additional amounts of Bi and Nb. The electrical conductivity increased while the Seebeck coefficient decreased as the amount of Bi and Nb was increased to x = y = 0.08. Consequently, the thermoelectric properties of $Ca_{0.96}Bi_{0.04}Mn_{0.96}Nb_{0.04}O_3$ improved nearly twofold over un–doped $CaMnO_3$.

Lemonnier (Lemonnier et al., 2010, pp.887–891) prepared $Ca_{3.95}RE_{0.05}Mn_3O_{10}$ (RE = Ce, Nd, Sm, Eu, Gd, Dy) by the SSR method. They reported that the electron concentration increased with substitute RE^{3+}. In addition, the electrical resistivity and Seebeck coefficient decreased and exhibited metallic behavior. The thermal conductivity of RE = Ce and Dy was lower than RE = Nd, Sm, Eu, and Gd at room temperature. The ZT value of RE = Ce, Nd, Sm, Eu, Gd, and Dy are 3.91, 4.09, 4.94, 5.83, 2.64, and 5.38, respectively at room temperature.

Linh (Linh et al., 2010, pp.2–5) calculated the electronic structure of $R_{0.25}Ca_{0.75}MnO_3$ (R = rare earth) using density functional theory (DFT) with a Dmol3 code. They reported that $CaMnO_3$ has a band gap of 1.034 eV (DFT+Dmol3) and G–AFM, and a small gap with doping rare earth. The $Eu_{0.25}Ca_{0.75}MnO_3$ exhibits the strongest structural change, as shown in Figure 12 and 13.

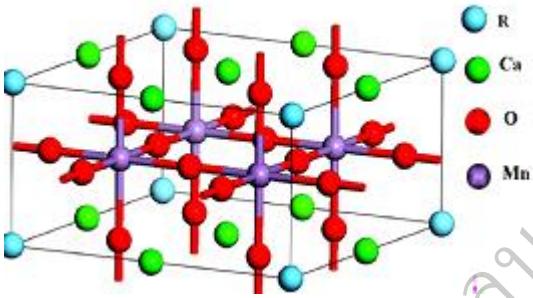

Figure 12 The $R_{0.25}Ca_{0.75}MnO_3$ cluster atoms

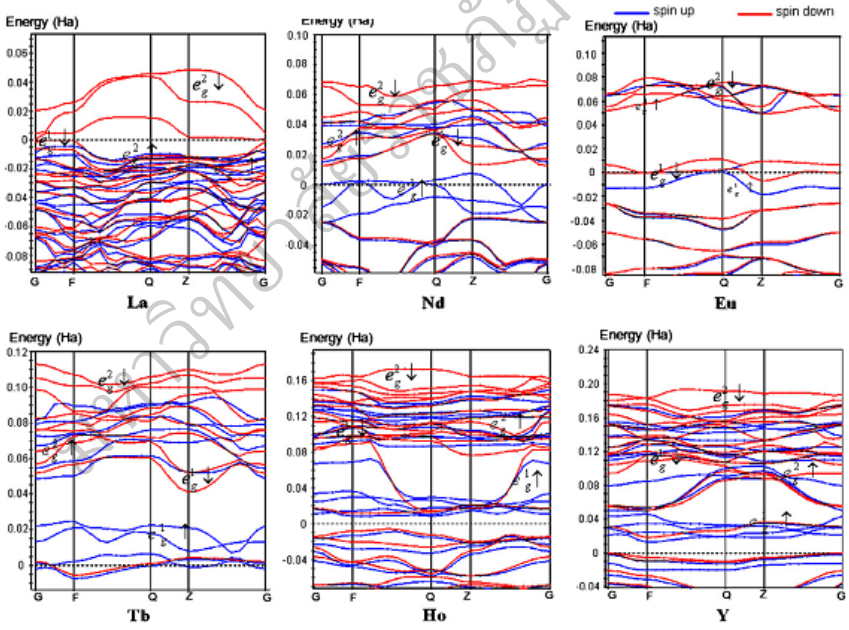

Figure 13 Energy band structure for the $R_{0.25}Ca_{0.75}MnO_3$ systems

(R = La, Nd, Eu, Tb, Ho, Y)

Kafash (Kafash, Moghadam, Kompany & Hosseini, 2010, unpage) prepared $CaMnO_3$ by the sol–gel method. They reported that $CaMnO_3$ has an orthorhombic structure and exhibits an electrical resistivity of 7 Ω cm at 325 K, decreasing to 2.25 Ω cm at 540 K.

Zhang (Zhang et al., 2011, pp.542–545) calculated electronic structure of $CaMnO_3$ using density functional theory (DFT). They reported that G–type AFM is more stable (via total energy minimization calculations). The band gap 0.7 eV was carried out by energy the band structure, as shown in Figure 14. The calculated of density state (DOS) exhibited Mn–*d* and O–*p* orbitals, which also analyzes electron mobility and carrier concentration as well as determining the thermoelectric properties.

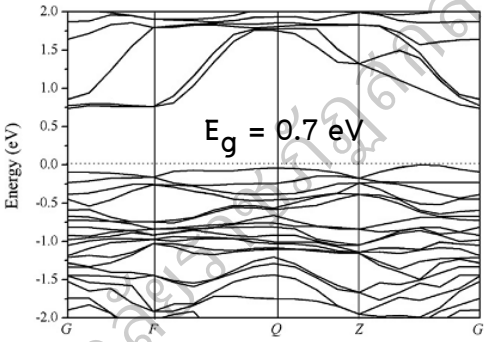

Figure 14 Energy band structure of $CaMnO_3$ calculated by DFT

Zhang (Zhang et al., 2011, pp.4171–4175) calculated the electronic structure of $Ca_{0.875}M_{0.125}MnO_3$ (M = Na, Ga) by DFT. They reported that the calculated energy band structure exhibits metallic characteristics (shown in Figure 15). The Debye temperature and phonon sound velocity also increased due to Na– and Ga–doped, respectively. The calculated phonon thermal conductivity exhibited was greater for Na–doped than Ga–doped. The Seebeck coefficient also appeared more enhanced with Na–doped as opposed to Ga–doped.

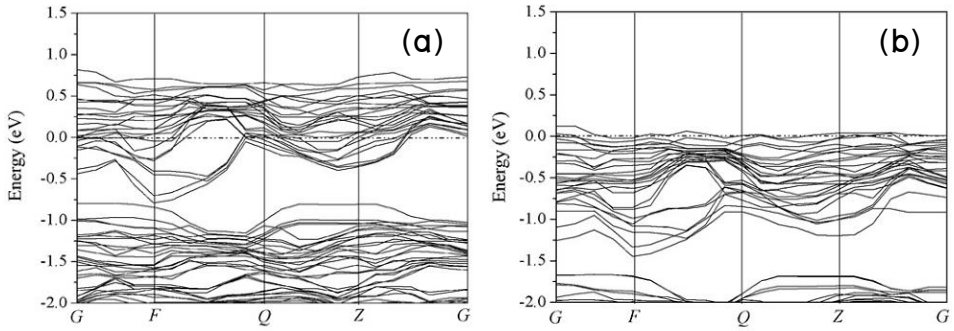

Figure 15 Energy band structure of (a) $Ca_{0.875}$ $Na_{0.125}MnO_3$ and (b) $Ca_{0.875}$ $Ga_{0.125}MnO_3$

Zhang (Zhang et al., 2011, pp.1258–1262) calculated the electronic structure of $Ca_{0.875}Sr_{0.125}MnO_3$ by DFT. They reported that the band gap decreased from 0.7 eV to 0.2 eV at Sr–doped, as shown in Figure 16(a). the density of state near the Fermi energy indicated that the Seebeck coefficient, carrier concentration and phonon resistance were also are enhanced, as show in Figure 21(b).

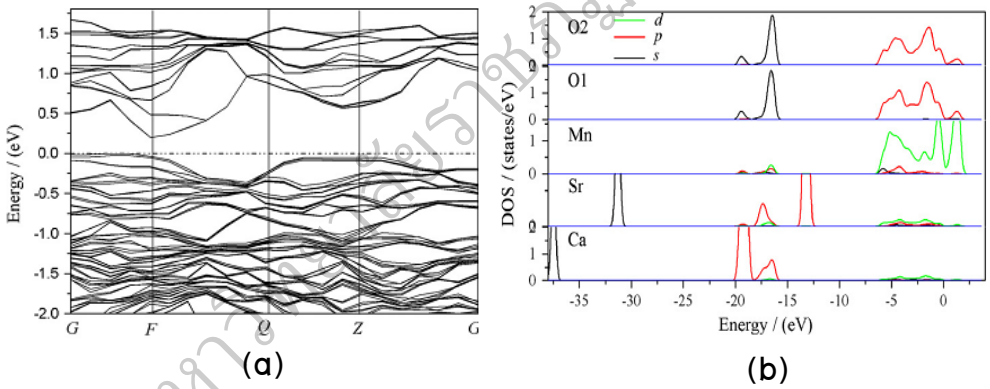

Figure 16 (a) Energy band structure and (b) partial density of state of $Ca_{0.875}Sr_{0.125}MnO_3$

Trang (Trang et al., 2011, pp.3613–3621) performed calculation on $CaMnO_3$ using DFT with Dmol3 code. They reported that $CaMnO_3$ has structure space groups P4/mmm and Pm–3m at the A–AFM phase, Pm–3m at B–, F– and G–FM; P4/mmm at C–, D– and E–AFM. In addition, at non–magnetic has structure space group Pm–3m.

Zhang (Zhang et al., 2013, pp.1859–1864) calculated the electronic structure of $CaMnO_3$, electrical conductivity, and Seebeck coefficient by way of DFT and Boltzmann theory, as shown in Figure 17. They reported that $CaMnO_3$ was stable at G–AFM with a band gap of 0.7 eV. The electrical conductivity exhibited good conductance along the a– and c–axes. The Seebeck coefficient was larger at the b–axis than it was at the a– and c–axes. The ZT value was calculated as 1.15 at 1000 K.

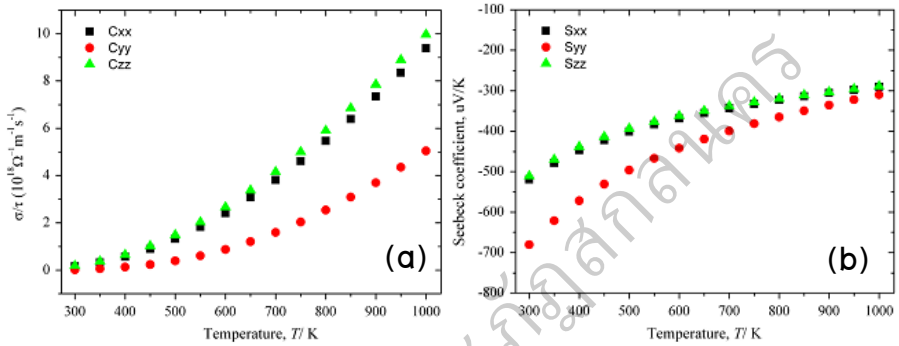

Figure 17 Calculated of (a) electrical conductivity and (b) Seebeck coefficient for $CaMnO_3$ versus temperature

Thongsri (Thongsri et al., 2013, pp.327–330) prepared CNTs–added $CaMnO_3$ (CNTs = 2%, 4%, 6%, 8% and 10%) by the SSR method. They reported that CNTs can reduce thermal conductivity of $CaMnO_3$ from 2 W m^{-1} K^{-1} to 0.5 W m^{-1} K^{-1}, as show in Figure 18.

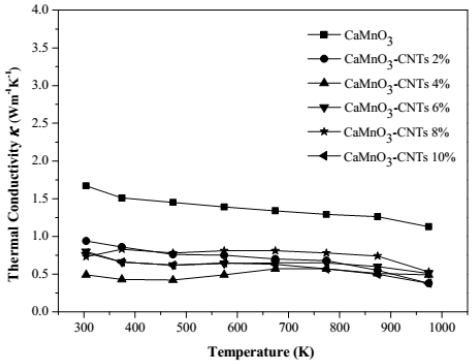

Figure 18 Thermal conductivity of CNTs–added $CaMnO_3$ versus temperature

Feipeng (Feipeng et al., 2013, pp.885–890) prepared $Ca_{1-X}Pr_XMnO_3$ (X = 0, 0.06, 0.08, 0.1, 0.12, 0.14) using the citrate–sol–gel method. They reported that carrier concentration and carrier mobility were increased, whilst the electrical resistivity and Seebeck coefficient were decreased with x content. The electrical resistivity, Seebeck coefficient and thermal conductivity all were increased at high temperature with these samples. The sample $Ca_{0.92}Pr_{0.08}MnO_3$ exhibited a ZT value of 0.16 at 873 K.

Mouyane (Mouyane et al., 2014, pp.71–77) prepared $Ca_{1-X}R_XMnO_3$ (R = Yb, Dy, Sm, Bi; X = 0, 0.1) by the flash combustion method. They reported that the valence of Mn was a hybrid of +4 and +3 which caused an increase in the unit cell volume, which in turn increased the ion radius of Yb–, Dy–, Sm–, and Bi–doped. Electrical resistivity and the Seebeck coefficient were decreased by Yb–, Dy–, Sm–, and Bi–doped. Metallic behavior was exhibited because the carrier concentration had increased. Moreover a good power factor was shown with a value of 165 $\mu W\ m^{-1}\ K^{-2}$ at 673 K for $Ca_{0.9}Yb_{0.1}MnO_3$

Seetawan (Seetawan, 2014, pp.9–14) calculated the thermoelectric properties of $Ca_{0.8}M_{0.2}MnO_3$ (M=Cu, Ag and Bi) using the DV–Xα method, MD method, and Maxwell–Boltzmann distribution model. He reported that the energy band structure exhibited a band gap of 0.68 eV which decreased to 0.18 eV, 0.11 eV and 0.42 eV for Cu–, Ag– and Bi–substitute. The electrical resistivity and Seebeck coefficient decreased due to an increase in the carrier concentration, as shown in Figure 19. The thermal conductivity decreased with Cu–, Ag– and Bi–substitutes, which indicates that good thermoelectric properties where present, as shown in Figure 20.

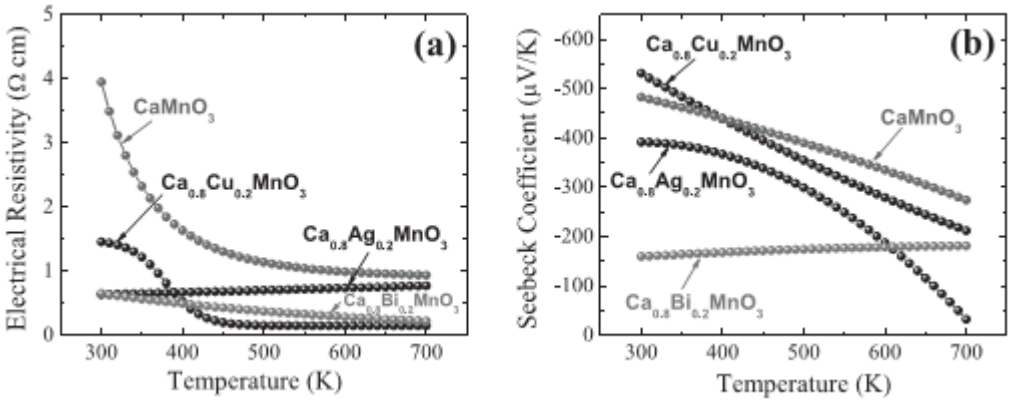

Figure 19 (a) Electrical resistivity and (b) Seebeck coefficient of $Ca_{0.8}M_{0.2}MnO_3$ M=Cu, Ag and Bi) versus temperature

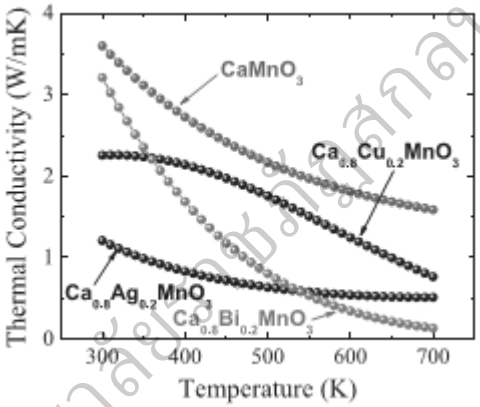

Figure 20 Thermal conductivity of $Ca_{0.8}M_{0.2}MnO_3$ (M=Cu, Ag and Bi) versus temperature

Zhu (Zhu et al., 2014, pp.15531–15536) prepared $Ca_{0.96}Dy_{0.02}RE_{0.02}MnO_3$ (RE = Ho, Er, Tm) by the SSR method. They reported that the unit cell volume increased because Mn^{4+} gives a carrier of Ho^{3+} (radius = 1.015 Å) Er^{3+} (radius = 1.004 Å) and Tm^{3+}(radius = 0.994 Å). The density of state per carrier concentration exhibited 0.184, 0.132, 0.144 and 0.125 for $Ca_{0.96}Dy_{0.02}MnO_3$, $Ca_{0.96}Dy_{0.02}Ho_{0.02}MnO_3$, $Ca_{0.96}Dy_{0.02}Er_{0.02}MnO_3$, and $Ca_{0.96}Dy_{0.02}Tm_{0.02}MnO_3$, respectively. The Seebeck coefficient exhibited an independent temperature, which indicates that the conduction band is near Fermi energy and less than k_BT. The electrical resistivity decreased with Ho–, Er– and Tm–doped. The ZT value was

measured as 0.225 at 1000 K for both $Ca_{0.96}Dy_{0.02}$ $Ho_{0.02}MnO_3$ and $Ca_{0.96}Dy_{0.02}$ $Er_{0.02}MnO_3$.

Villa (Villa et al., 2014, pp.22–25) prepared $Ca_{0.95}La_{0.05}$ $Mn_{1-X}Nb_XO_3$ ($0 \leq x \leq 0.10$) by the SSR method. They reported that the unit cell volume increased with x content. The bond length of Mn^{4+}–O–Mn^{4+}change to Mn^{4+}–O–Mn^{3+} as Nb^{5+}–doped. The electrical resistivity and Seebeck coefficient exhibited metallic behavior. The thermoelectric performance of the sample x=0.03 can be enhanced by a power factor of 0.4 $\mu W\ cm^{-1}\ K^{-2}$ at 300 K.

Zhu (Zhu et al., 2015, pp.1535–1539) prepared $Ca_{1-2X}Dy_XYb_XMnO_3$ ($0 \leq x \leq 0.1$) by the SSR method. They reported that the valence of Mn^{4+} changed to Mn^{3+} because Mn^{4+} was given an electron from Dy and Yb. The electrical resistivity, Seebeck coefficient and thermal conductivity decrease with Dy– and Yb–doped. The sample also indicated metallic behavior. The ZT value was 0.27 at 1073 K for sample x = 0.02, which demonstrated good thermoelectric performance by double–doped.

Zhu (Zhu et al., 2015, pp.105–109) prepared $Ca_{0.98}Dy_{0.02}Re_{0.02}MnO_3$ (Re = La, Pr, Sm, Er, Ho, Yb) by the SSR method. They reported that the electrical resistivity and Seebeck coefficient decreased due to an increase in the carrier concentration and carrier mobility. The thermal conductivity was decreased due to a shortage of phonon vibration. The ZT value was 0.25 at 973 K for $Ca_{0.96}Dy_{0.02}Yb_{0.02}MnO_3$ which exhibited an enhanced thermoelectric performance.

Kabir (Kabir et al., 2015, pp.347–351) prepared $Ca_{1-X}Bi_XMnO_3$ (X = 0, 0.02, 0.03, 0.04, 0.06, 0.10) by the SSR method. They reported that the electrical resistivity and Seebeck coefficient decreased with an increase in x (according to the carrier concentration). Thermal conductivity decreased at x = 0.03 and 0.04. The ZT value was 0.25 at 973 K for x = 0.03. A small Bi–doped enhanced the TE performance of $CaMnO_3$.

Zhang (Zhang et al., 2015, pp.1–5) calculated the electronic structure and thermoelectric properties of $Ca_{0.75}R_{0.25}MnO_3$ (R = La, Ce, Pr, Nd, Pm, Sm, Gd, Tb, Dy, Ho, Er, Tm, Lu) by using both the DFT and Boltzmann theory. They reported that

$CaMnO_3$ was stable at G–AFM, whereas the substitution of Lanthanides produced greater stablility at C–AFM. The energy band structure exhibited a Fermi energy shift upwards into the conduction bands, which indicates that doped systems become metallic, as shown in Figure 21. Confirmation that Mn^{4+} was given an electron form Lanthanides was confirmed by the unit cell volume, difference of charge electron Mn/R and binding energy. The Seebeck coefficient and electrical conductivity also showed that Lanthanides can be used to enhance thermoelectric performance and metal behavior, as shown in Figure 22.

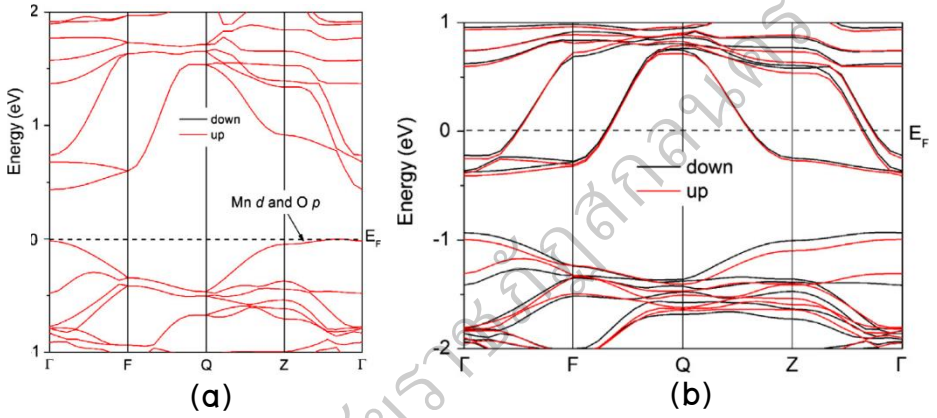

Figure 21 Energy band structure C–AFM of (a) $CaMnO_3$ and (b) $Ca_{0.75}R_{0.25}MnO_3$ (R = La, Ce, Pr, Nd, Pm, Sm, Gd, Tb, Dy, Ho, Er, Tm, Lu)

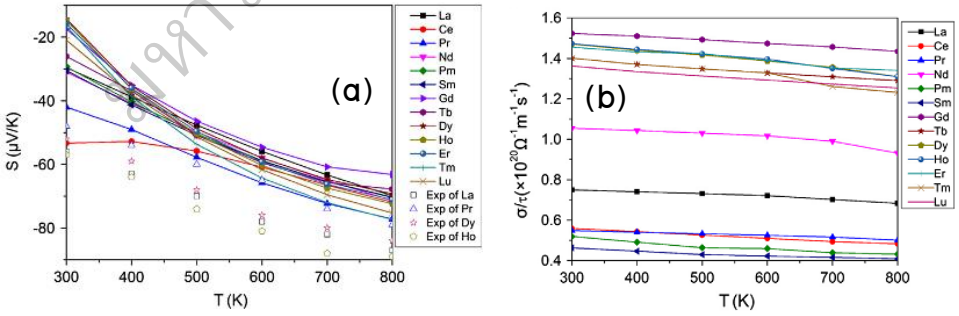

Figure 22 (a) Seebeck coefficient and (b) electrical conductivity of $Ca_{0.75}R_{0.25}MnO_3$ (R = La, Ce, Pr, Nd, Pm, Sm, Gd, Tb, Dy, Ho, Er, Tm, Lu) versus T

For the period 1995 – 2015, the development of the Dimensionless figure of merit for $CaMnO_3$ is illustrated in Figure 23;

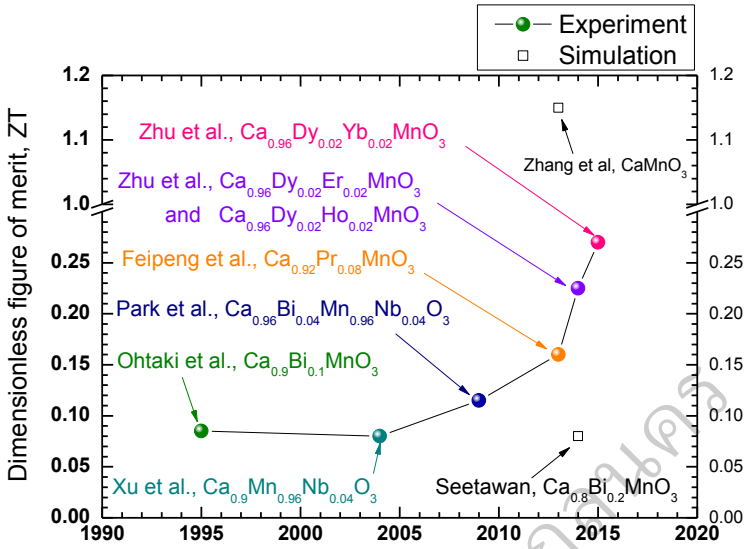

Figure 23 History of ZT for $CaMnO_3$ thermoelectric material

In addition, there has been much research in the use of CNTs to enhance the performance of oxide thermoelectric materials composed of TiO_2 and $Ca_3Co_4O_9$.

Lai (Lai et al., 2015, p. 8120–4) prepared the CNTs/TiO_2 (CNTs = multi-walled CNTs, MWCNTs) by the spark plasma sintering (SPS) technique at 1200 K. Then they simulated the electronics structure of CNTs/TiO_2 by the DFT method, based on an ab initio simulation, as shown in Figure 24. They reported that CNTs/TiO_2 showed increased electrical conductivity and Seebeck coefficient, while thermal conductivity simultaneously decreased. With regard to the energy band structure, carbon can reduce the band gap from 2.89 eV to 1.67 eV, which corresponded to with the experimental data, as show in Figure 25. The ZT value illustrated that MWCNTs can be used to enhance thermoelectric performance, as shown in Figure 26.

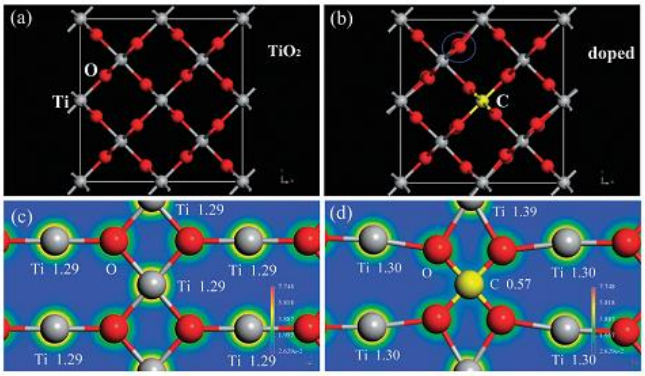

Figure 24 The ab initio simulated structure of (a) TiO_2 and (b) carbon doped TiO_2, the Mulliken charge dispersion of (c) TiO_2 and (d) carbon doped TiO_2

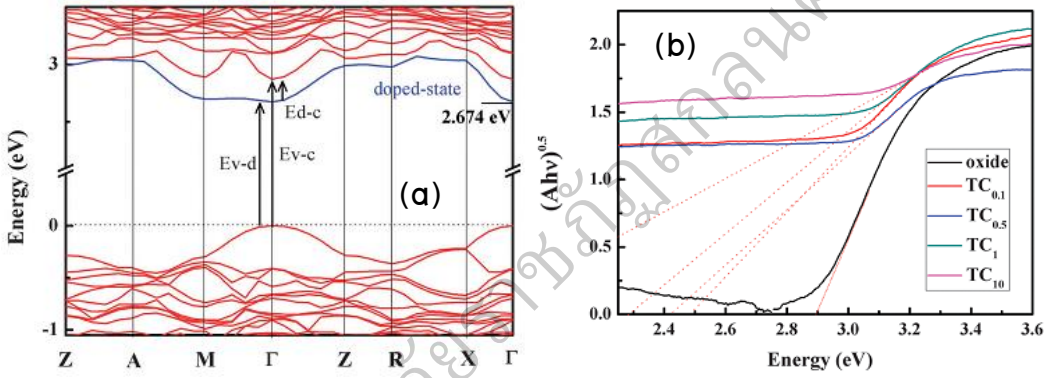

Figure 25 (a) The energy band structure of TiO_2 and carbon doped TiO_2 and (b) UV-vis spectra of TiO_2 and carbon doped TiO_2

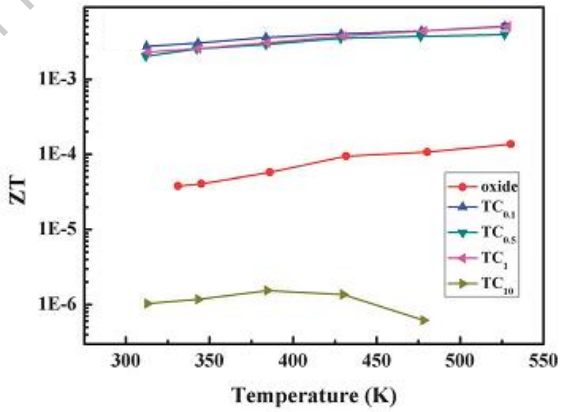

Figure 26 Dimensionless figure of merit of TiO_2 and carbon doped TiO_2

Tang (Tang et al., 2015, pp.961–965) prepared CNTs doped $Ca_3Co_4O_9$ by the sol–gel method. They reported that CNTs can reduce thermal conductivity from 1 W m^{-1} K^{-1} to 0.319 W m^{-1} K^{-1} at room temperature. CNTs can also enhance the Seebeck coefficient form 50 μV K^{-1} to 125 μV K^{-1} at room temperature. Electrical resistivity was increased by CNTs–doped but CNTs however, did not enhance electrical resistivity. CNTs did not improve the ZT of $Ca_3Co_4O_9$. The thermal conductivity, Seebeck coefficient and electrical resistivity is shown in Figures 27 and 28;

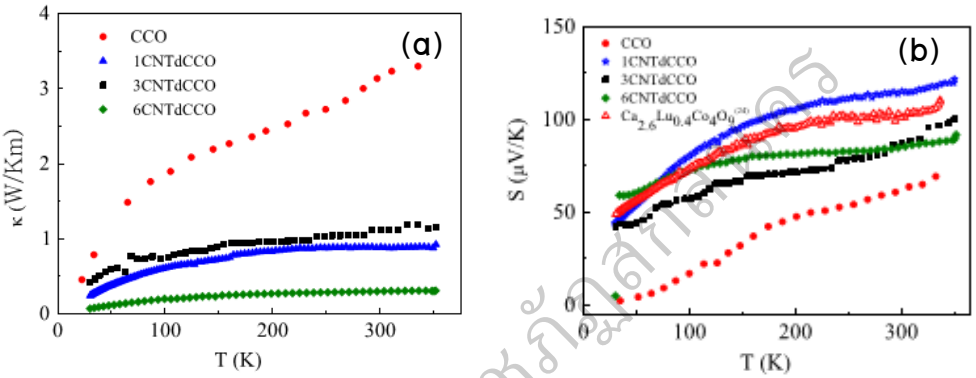

Figure 27 (a) Thermal conductivity and (b) Seebeck coefficient for xCNTdCCO samples versus temperature.

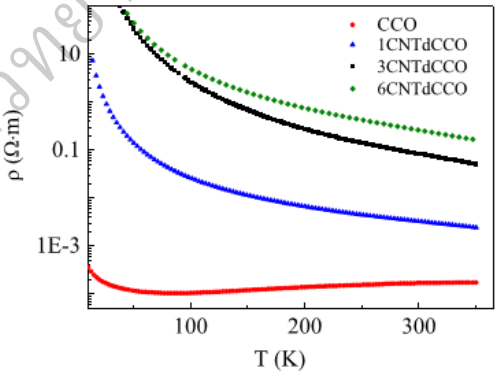

Figure 28 Electrical resistivity for xCNTdCCO samples versus temperature.